

Automatic Detection of Microcalcification in Mammograms– A Review

K.Thangavel¹, M.Karnan^{2*}, R.Sivakumar³, A. Kaja Mohideen³

1: Department of Mathematics, Gandhigram Rural Institute-Deemed University,

2: Department of computer science, Gandhigram Rural Institute-Deemed University,

Gandhigram-624302, Tamil Nadu, India. Email: karnanme@yahoo.com fax:91-4551-227229

3: Department of Computer Science and Engineering, R.V.S.College of Engineering & Technology, Dindigul, Tamil Nadu, India.

Abstract

In this review paper, it is intended to summarize and compare the methods of automatic detection of microcalcifications in digitized mammograms used in various stages of the Computer Aided Detection systems (CAD). In particular, the pre processing and enhancement, bilateral subtraction techniques, segmentation algorithms, feature extraction, selection and classification, classifiers, Receiver Operating Characteristic (ROC); Free-response Receiver Operating Characteristic (FROC) analysis and their performances are studied and compared.

Keywords: Mammography, Microcalcification, Image Enhancement, Segmentation, Feature extraction.

1. Introduction

Breast cancer is one of the major causes for the increase in mortality among women, especially in developed and under developed countries. The World Health Organization's International agency for Research on Cancer in Lyon, France, estimates that more than 150 000 women worldwide die of breast cancer each year. The breast cancer is one among the top three cancers in American women. In United States, the American Cancer Society estimates that, 215 990 new cases of breast carcinoma has been diagnosed, in 2004. It is the leading cause of death due to cancer in women under the age of 65 [121]. In India, breast cancer accounts for 23% of all the female cancers followed by cervical cancers (17.5%) in metropolitan cities such as Mumbai, Calcutta, and Bangalore. However, cervical cancer is still number one in rural India. Although the incidence is lower in India than in the developed countries, the burden of breast cancer in India is alarming. Organ chlorines are considered a possible

cause for hormone-dependent cancers [119]. Detection of early and subtle signs of breast cancer requires high-quality images and skilled mammographic interpretation. In order to detect early onset of cancers in breast screening, it is essential to have high-quality images. Radiologists reading mammograms should be trained in the recognition of the signs of early onset of, which may be subtle and may not show typical malignant features. Mammography screening programs have shown to be effective in decreasing breast cancer mortality through the detection and treatment of early onset of breast cancers.

Emotional disturbances are known to occur in patient's suffering from malignant diseases even after treatment. This is mainly because of a fear of death, which modifies Quality Of Life (QOL) [105]. Desai et al., [34] reported an immunohistochemical analysis of steroid receptor status in 798 cases of breast tumors encountered in Indian patients, suggests that breast cancer seen in the Indian population may be biologically different from that encountered in western practice. Most imaging studies and biopsies of the breast are conducted using mammography or ultrasound, in some cases, magnetic resonance (MR) imaging [66]. Although by now some progress has been achieved, there are still remaining challenges and directions for future research such as [20] developing better enhancement and segmentation algorithms.

1.1 Commercial CAD System

It is generally believed that CAD can provide a valuable second look and improve the accuracy of breast cancer detection at an earlier stage [121]. The typical CAD system consists of two freestanding units: a processing unit that digitizes and analyzes the film images, and a display unit consisting of a dedicated mammography viewer equipped with monitors that

display low spatial resolution digital images of the examination. The digital images are linked by a barcode to the panels where the films are mounted and are displayed by pressing a button on the auto-viewer control panel. Each digital image may contain zero to several marks indicating areas where the detection algorithm recognize a pattern that warrants evaluating by the radiologist. Two different types of marks typically used – asterisks [*] indicating masses or architectural distortions or triangles [Δ] indicating microcalcifications (these marks will be different for the various computer-aided detection system).

CAD has been used as a research tool since 1999. Initial retrospective work performed by evaluating prior screening mammograms of patients whom had a cancer detected at a subsequent screening mammogram. These mammograms were digitized and analyzed with CAD. It is found that although the mammograms are double read, there was room for improvement in cancer detection by implementing CAD.

A. Lauria et al., [74] described the CAD systems are: the Second Look (CADx Medical Systems, Canada) commercial system and the Computer Assisted Library in Mammography (CALMA) research CAD system. Two different CAD systems were considered: a commercial system and a research one. The former is the Second Look (CADx, Medical Systems) produced in Canada. It is a three-step system. First, it digitizes mammograms (at $45\mu\text{m}$ sampling aperture, 12 bit/pixel) and then a neural network analyses the image data to produce, as a last step, a printed output (the Mammography), where potential lesions are pointed out by markers. An oval mark indicates a massive lesion, while a rectangular mark points to a cluster of microcalcifications. The system indicates at most three markers for microcalcification cluster in each image. The time necessary to obtain four printed reports for each subject is about 6 min. It is not possible to modify, to visualize or to store the images obtained. The radiologist uses the printed images as an alternative support, while making the diagnosis uses the original mammograms.

The latter CAD system used was CALMA. This research system has been developed as a part of the research project funded by Istituto Nazionale di Fisica Nucleare (INFN) and carried out in collaboration with several Italian universities and hospitals. The hardware consists of a personal computer and of a linear Charge Coupled Device (CCD) film scanner. The original software developed runs under the UNIX operating system. CALMA first digitizes the mammogram ($85\mu\text{m}$, 12 bit/pixel) and then saves the (10 Mbytes) corresponding file in a special format.

1.2 Digital Equipment

Antony Jalink et al., [4] presented a novel technique for large-field digital mammography. This instrument uses a mosaic of electronic digital imaging CCD arrays, novel area scanning, and a radiation exposure and scatter reducing mechanism. The imaging arrays are mounted on a carrier platform in a checkerboard pattern mosaic. To fill in the gaps between array active areas the platform is repositioned three times and four X-ray exposures are made. The multiple image areas are then recombined by a digital computer to produce a composite image of the entire region. To reduce X-ray scatter and exposure, a lead aperture plate is interposed between X-ray source and patient. The aperture plate has a mosaic of square holes in alignment with the imaging array pattern and the plate is repositioned in synchronism with the carrier platform. They discussed proof-of-concept testing demonstrating technical feasibility of their approach. The instrument should be suitable for incorporation into standard mammography units. Unique features of the new techniques are: large field coverage ($18 \times 24\text{ cm}$); high spatial resolution (14-17 lp/mm); scatter rejection; and excellent contrast characteristics and lesion detectability under clinical conditions.

The CAD mammography systems for microcalcification detection have gone from crude tools in the research laboratory to commercial systems. Several commercial companies such as R2 Technology Inc., Hewlett Packard Co., Sterling Diagnostic Imaging, Siemens, GE, Med Detect/Lockheed Martin, were developing or designing mammography systems for clinical applications. R2 Technology Inc. has produced a system ImageCheckerJ for microcalcifications and mass detection. (www.r2tech.com)

2. Database (Image Acquisition)

To access the real medical images for carrying out the tests is a very difficult due to privacy issues and heavy technical hurdles. X-ray film mammogram is converted into digital mammograms. Laser scanners are used to digitize conventional film mammograms by measuring the Optical Density (OD) of small windowed regions of film and converting them to pixels with a grey level intensity. The size of the window determined the spatial resolution of the digitized image. The resolution is typically expressed in units of microns per pixel, indicating the size of the square region of film that each pixel in the digitized image represents. Each pixel location on the film is illuminated with a beam of known intensity (photon flux density). The exact pixel value depends on the range of optical densities that the scanner is capable of measuring and the number of bits used to store the grey level of each pixel. The accuracy of computer detection schemes on digital mammograms will depend partially on the spatial resolution and range of grey levels at which the images are digitized. For

example, clinically important microcalcifications can be as small as 0.1mm (100 microns) or smaller. In order for calcifications this small to appear in a digitized image, a resolution would be needed for these small calcifications to occupy more than a single pixel in the image. This in turn would make them easier to detect and easier to distinguish from noise.

2.1 MIAS

The Mammography Image Analysis Society (MIAS), which is an organization of UK research groups interested in the understanding of mammograms, has produced a digital mammography database (<ftp://peipa.essex.ac.uk>). The data used in these experiments was taken from the MIAS. The X-ray films in the database have been carefully selected from the United Kingdom National Breast Screening Programme and digitized with a Joyce-Lobel scanning microdensitometer to a resolution of $50 \mu\text{m} \times 50 \mu\text{m}$, 8 bits represent each pixel. The database contains left and right breast images for 161 patients, is used. Its quantity consists of 322 images, which belong to three types such as Normal, benign and malignant. There are 208 normal, 63 benign and 51 malignant (abnormal) images.

3. Bilateral Subtraction

The mammogram images may be time sequences of the same breast from two different screening examinations, or they may be bilateral images of the left and right breasts obtained during the same examination. Advances in the area of computerized image analysis applied to mammography may have very important practical applications in automatically detecting asymmetries (masses, architectural distortions, etc.) between the two breasts. This section discusses various techniques for extracting suspicious regions from background tissue.

3.1 Border Detection and Nipple Identification

Mendez et al., [87] developed a fully automatic technique to detect the breast border and the nipple, this being a prerequisite for further image analysis. To detect the breast border, an algorithm that computes the gradient of gray levels was applied. First, a smoothed version of the entire mammogram was computed. This low-frequency image was generated by replacement of the pixel value with a mean pixel value computed over a square area of 11×11 pixels centered at the pixel location. In a profile of a line across the mammogram is plotted, without any transformation, the result is an irregular line, where several local maxima appear. The result of using a smoothed version of the original image produces a plot with regular shape. The presence of the local maxima disappears. Next, five points, (x_1, y_1) , (x_2, y_2) , (x_3, y_3) , (x_4, y_4) , (x_5, y_5) , were automatically selected as reference points to divide the breast into three regions (I, II and III). Finally, a tracking algorithm was applied to the mammogram to detect the border. A point (x, y) would belong to the border if the gray level

value $(f(x_i, y_i))$ of the nine previous pixels verifies the condition:

$$f(x_1, y_1) < f(x_2, y_2) < \dots < f(x_7, y_7) \leq f(x_8, y_8) \leq f(x_9, y_9) \leq f(x, y)$$

This is called the tracking algorithm. There is a relationship between the regions and the tracking process: in region I the algorithm searches the breast border from left to right; in region II the algorithm searches the border from top to bottom; and finally in III the algorithm searches the border from right to left.

To detect the nipple, three algorithms were compared (maximum height of the breast border, maximum gradient, and maximum second derivative of the gray levels across the median-top section of the breast). This will be useful in the development of CAD schemes in digital mammography to automatically distinguish between normal and abnormal cases, and in turn, aid the radiologist in the mammographic screening.

3.2. Active Contours (Snake algorithm)

Michael Wirth [91] has explored the application of active contours to the problem of extracting the breast region in mammograms. Method for mammogram segmentation: (i) the breast-air interface itself is a very low gradient and may be obscured by noise; (ii) the uncompressed fat near the breast-air interface is a gradient, growing as the fat nears the center of the breast. The method will have to include some sort of noise removal to allow the snake to distinguish between the breast contour and the noise in the mammogram. Snakes are designed to fill in gaps which occur in contours, so are well suited to dealing with contour detail which is lost during the process of noise removal. From observation (ii), two points can be inferred. First, right-to-left edge detection will pick up the gradient of the breast as an edge when the breast is approaching from the left. In contrast, left-to-right edge detection will not pick up the breast contour but will pick up noise and other artifacts. Secondly, a dual threshold would produce a difference in terms of the breast area detected. By taking this difference, one should be able to obtain an approximate location of the breast contour.

Ruey-Feng Chang et al., [113] developed a method to use the three-dimensional (3-D) snake technique to obtain the tumor contour for the pre- and the post-operative malignant breast excision by the vacuum assisted biopsy instrument Mammotome. This technique of assessing the margin of two can help the physician to evaluate the effect of the surgery. By using the isotropic diffusion filter, the noise and speckles can be reduced. Then the stick detection is adopted for enhancing the edge. Finally, the gradient vector flow (GVF) snake is used to obtain the tumor contour. These techniques are extended to the 3-D techniques to increase the accuracy and robust of segmentation

results. This study can help physicians to improve the minimal invasive operation for a breast tumor.

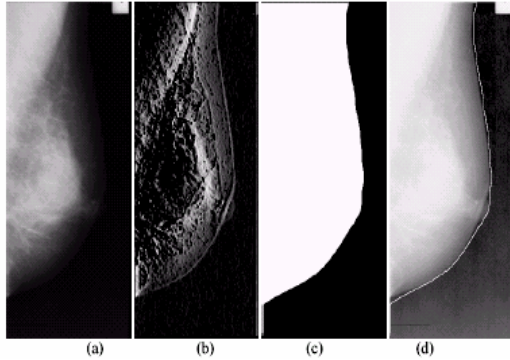


Figure 3.1 an example of breast region segmentation performed on an MIAS mammogram: (a) Original Mammogram; (b) Enhanced Image; (c) Extracted Breast Region; (d) Contour overlay on a LOG-attenuated version of (a).

3.3. Extraction of Suspicious Region using Spatial Filtering Technique

An input mammogram is processed with two spatial filters to obtain a signal-enhanced image and a signal-suppressed image. By subtracting the suppressed image from the enhanced image, a difference-image is obtained. As the structure of normal breast tissue is the same in the enhanced and suppressed images, this component will be reduced in the difference-image. The enhancement filter is a spatial filter that has been developed to approximately match the size and contrast variations of typical microcalcifications. However, for two reasons the filter is not a conventional matched filter: First, the frequency content of the normal background tissue (high frequency noise) was not taken into account in the design process. Second, due to the varying size and shape of microcalcifications, a simplified model, i.e. a square filter kernel was used. Based on an analysis of the two-dimensional profiles of some typical microcalcifications, the contrast variation of microcalcifications was approximated with different weighting factors for the filter. The enhancement filter provides an output measure of the correlation between the filter response function and the spatial variation of the image. Consequently, at the locations of microcalcifications, the peak values of pixels in the filtered image are increased relative to the pixel values of normal (background) tissue (Gulsrud, 2000).

3.4. Directional Filtering with Gabor Wavelets

Ferrari et al., [42] developed a procedure for the analysis of left-right (bilateral) asymmetry in mammograms. The procedure is based upon the detection of linear directional components by using a

multiresolution representation based upon Gabor wavelets. A particular wavelet scheme with two-dimensional Gabor filters as elementary functions with varying tuning frequency and orientation, specifically designed in order to reduce the redundancy in the wavelet-based representation, is applied to the given image. A 2-D Gabor function is a Gaussian modulated by a complex sinusoid. It can be specified by the frequency of the sinusoid and the standard deviations and of the Gaussian envelope as

$$\psi(x,y) = (1 / (2\pi \sigma_u \sigma_v)) \exp \{ -\frac{1}{2} [(x^2/\sigma_u^2) + (y^2/\sigma_v^2)] + 2\pi j Wx \} \dots\dots(1)$$

By means of “Gabor wavelet representation”, a bank of Gabor filters normalized to have dc responses equal to zero and designed in order to have low redundancy in the representation. The Gabor wavelets are obtained by dilation and rotation of $\psi(x,y)$ as in (1) by using the generating function

$$\begin{aligned} \Psi_{m,n}(x,y) &= a^{-m} \psi(x',y'), \quad a > 1, \quad m, n = \text{integers} \\ x' &= a^{-m} [(x-x_0) \cos \theta + (y-y_0) \sin \theta]; \\ y' &= a^{-m} [-(x-x_0) \sin \theta + (y-y_0) \cos \theta] \quad \dots\dots(2) \end{aligned}$$

where, (x_0, y_0) center of the filter in the spatial domain; $\theta = n\pi / K$; K total number of orientations desired; m and n scale and orientation, respectively. The scale a^{-m} factor in (2) is meant to ensure that the energy is independent of m . Equation (1) can be written in the frequency domain as

$$\psi(u,v) = (1 / (2\pi \sigma_u \sigma_v)) \exp \{ -\frac{1}{2} [((u-W)^2 / \sigma_u^2) + (v^2 / \sigma_v^2)] \} \dots(3)$$

where, $\sigma_u = 1 / \{2\pi\sigma_x\}$ and $\sigma_v = 1 / \{2\pi\sigma_y\}$. The design strategy used is to project the filters to ensure that the half-peak magnitude supports of the filter responses in the frequency spectrum touch one another. By doing this, it can be ensured that the filters will capture the maximum information with minimum redundancy.

The filter responses for different scales and orientation are analyzed by using the Karhunen-Loeve (KL) transform and Otsu’s method of thresholding. The KL transform is applied to select the principal components of the filter responses, preserving only the most relevant directional elements appearing at all scales. The selected principal components, thresholded by using Otsu’s method, are used to obtain the magnitude and phase of the directional components of the image. Rose diagrams computed from the phase images and statistical measures computed thereof are used for quantitative and qualitative analysis of the oriented patterns.

Table 1. Overview of Bilateral Subtraction

Methods	Results	Remarks
Gradient of gray levels, maximum height of the breast border, maximum gradient, and maximum second derivative of the gray levels [4]	89% correct rate. Out of 322 images from MIAS.	Useful in the development of CAD schemes in digital mammography to automatically distinguish between normal and abnormal cases.
Active contour, snake algorithm [91]	98.4% of correct and 1.6% of error rate of 25 images from MIAS	Fails to adequately segment the nipple when it is in profile in a mammogram.
Karhunen-Loeve (KL) transform and Otsu's method of thresholding, Gabor filters [42] [87]	74.4% were achieved from 80 images from MIAS database	The classification results are encouraging, considering the small number of features (first- and second-order angular moment and entropy) used to differentiate between normal and asymmetric mammograms.
Three-dimensional (3-D) snake technique [113]	50% correct rate, Suited for 2 out of four 3-D US datasets.	Used to obtain the tumor contour for the pre- and the post-operative malignant breast excision by the vacuum assisted biopsy instrument Mammotome.

4. Enhancement

The enhancement aspects are surveyed and analyzed in this section.

4.1. Preprocessing

Mudigonda et al. [94] described a method for the detection of masses in mammographic images that employs recursive Gaussian low pass filtering and sub sampling operations in a multiresolution-based pyramidal architecture as preprocessing steps to achieve the required level of smoothing of the image. The image is smoothed with a separable Gaussian kernel of width 15 pixels (1 pixel 200 μ m) and reduced to a maximum of 64 gray levels. A method is used to generate Gaussian kernels. Here, the width specified for a Gaussian kernel refers to the total width of its support and not the width at its half-maximum height. A map of iso-intensity contours is generated by thresholding the image using a threshold close to zero. From the map of iso-intensity contours, a set of closed contours is identified by employing chain code principles.

The next step in the algorithm is to threshold the image at varying levels of intensity to generate a map of iso-intensity contours. The purpose is to extract concentric groups of closed contours to represent the isolated regions in the image. The low-resolution image is initially reduced to 64 gray levels in intensity and thresholded at 30 different levels starting from the maximum intensity level 64, with a step-size decrement of 0.01. The above parameters are chosen based on the observation of histograms of several low-resolution images. The histogram of the low-resolution image obtained by way of preprocessing the image, the intensity level at which the masses and other dense tissues appear to merge with the surrounding breast parenchyma is observed to be the minimum threshold level of 44.

4.2 Conventional Enhancement Techniques

A complete survey on conventional enhancement technique is highlighted below.

4.2.1. Contrast Stretching

The simplest method of increasing the contrast in a mammogram is to adjust the mammogram histogram so that there is a greater separation between foreground and background gray-level distributions. Denoting the input image gray level by x , and the output grayscale values by y , the rescaling transformation is $y = f(x)$, where the $f(\cdot)$ can be any designing function. The following function shows a typical contrast stretching transformation of the gray-level distribution in the mammogram

$$y = \begin{cases} \alpha x, & 0 \leq x < a \\ \beta (x-a) & a \leq x < b \\ \gamma(x-b) & b \leq x < L \end{cases} \quad (1)$$

where, the slope α , β and γ are chosen greater than unity in the region of stretch, the parameters a and b can be obtained by examining the histogram of the original mammogram, and L is the maximum gray level of the original mammogram.

4.2.2. Histogram Equalization

Histogram modeling techniques modify an image so that its histogram has a desired shape. This is useful in stretching the low contrast levels of mammograms with narrow histograms. A typical technique in histogram modeling is histogram equalization. Let us consider the mammogram histogram as a probability distribution. Based on the information theory, the uniform distribution achieves the maximum entropy, which contains the most information. Therefore, redistribute the gray levels to obtain a histogram as uniform as possible, the mammogram information should be maximized.

4.2.3. Gradient Operators

Convolution masking is commonly used for mammography enhancement. The unsharp masking [16] and Sobel gradient operators are two examples. Dhawan et al. [35] used an optimal adaptive enhancement method to reduce the influence. One of the requirements of the contrast enhancement function is to provide 40°–50° slopes in the low input range (0–0.1) to reduce noise enhancement. The processed image is sharper because low-frequency information in the mammogram is reduced in intensity while high frequency details are amplified.

4.2.4. Fixed-Neighborhood Statistical Enhancement

The enhancement techniques stated above are global-based approaches. For some mammograms that contain inhomogeneous background, local-based enhancement techniques can have better performance. Local enhancement techniques use statistical properties in the neighborhood of a pixel to estimate the background, suppress it, and increase local contrast.

4.2.5. Adaptive Neighborhood Technique

The above techniques can all be classified as either fixed-neighborhood or global techniques. They may adapt to local features within a neighborhood, but do not adapt the size of the neighborhood to local properties. Many medical images, including mammograms, possess clinically defined image features within a region of interest. These features can vary widely in size and shape, and often cannot be enhanced by fixed-neighborhood or global techniques. Thus, there is a need for adaptive-neighborhood techniques, which adaptively change the size of regions in a given image and enhance the regions with respect to their local background. Region-based method can enhance detail that is more anatomical without significantly introducing artifacts, and has demonstrated that it can identify calcifications more effectively in the image of dense breasts where the contrast between calcifications and breast tissue is quite low [92].

4.2.6. Enhancement by Background Removal

To enhance the visibility and detectability of microcalcifications, background removal is considered a necessary procedure. Background removal is a direct method of reducing the slowly varying portions of an image, which in turn allows increased gray-level variation in image details. It is usually performed by subtracting a low pass filtered version of the image from itself. Morphological processing and partial wavelet reconstruction are two methods of estimating the image background that have been used successfully for this purpose.

Mammograms are reconstructed from wavelet coefficients modified at one or more levels by local and global nonlinear operators [73]. An adaptive mammographic enhancement using first derivative and local statistics was studied [68]. A pattern-dependent

enhancement algorithm based on the fractal-modeling scheme was studied [51,80]. Comparing with microcalcifications, the breast background tissues have high local self-similarity, which is the basic property of fractal objects.

4.3. Non-Linear Filter

Lai et al. [117] presents a method uses modified median filtering to enhance mammogram images. a modification of median filtering, with respect to their performance in enhancing mammogram images. Edge-preserving smoothing tries to search for a homogeneous neighborhood in different directions of a given pixel and averages in this neighborhood only. Half-neighborhood method operates as un-weighted averaging at pixels in the interior of a region. In the k-nearest neighbor method, is based on the idea that pixels in the same region should have similar gray values. Directional smoothing is similar to the half-neighborhood method in that for pixels in the interior of a region, averaging is done using all neighborhood pixels. One disadvantage of this method is the high computational cost. A coarse-fine template matching method was implemented, and the results show that the computational cost of the method can be reduced by such an approach.

Qian et al. [136] designed a new class of nonlinear filters with characteristics for noise suppression and detail preservation is for processing digital mammographic images. First, the noise-suppressing properties of the tree-structured filter were compared to single filters, namely the median and the central weighted median with conventional square and variable shape adaptive windows; simulated images were used for this purpose. Second, the edge detection properties of the tree-structured filter cascaded with the dispersion edge detector were compared to the performance of the dispersion edge detector alone, the Sobel operator, and the single median filter cascaded with the dispersion edge detector.

A property of the weighted median filter is that, as more emphasis is placed on the central weights, its ability to suppress noise decreases and its ability to preserve image detail increases. The weighted median filter with only a single central weight is called Central Weighted Median Filter (CWMF). The output $Y(i,j)$ of a CWMF with an odd size window is given by:

$$Y(i,j) = \text{median} \{X(i-s,j-t), 2K \text{ copies of } X(i,j), (s,t) \in W\}$$

In the case of a single filter, the orientation of these windows can be adaptively changed pixel by pixel according to the different curve features in an image leading to an operator and image independent process. In a Tree-Structured Filter (TSF) with N stages, the first stage of the filter consists of a number of CWMFs equal to the number of n of different shape windows; the original unfiltered signal $X(i,j)$ was used as a single input to each sub filter. The second stage of the filter

consists of fewer CWMFs; their number m depends on the particular architecture. Their inputs are combinations of an even number of CWMF outputs from the first stage and the original signal $X(i,j)$. Several intermediate stages can be added by repeating the above procedure and decreasing the number of CWMFs every time.

4.4. Adaptive Enhancement

Kim et al. [68] described an adaptive image enhancement method for mammographic images, which is based on the first derivative and the local statistics. The adaptive enhancement method consists of three processing steps. (a) Remove the film artifacts that may be misread as microcalcifications. (b) Compute the gradient images by using the first derivative operators. (c) Enhance the important features of the mammographic image by adding the adaptively weighted gradient images. Local statistics of the image are utilized for adaptive realization of the enhancement, so that image details can be enhanced and image noises can be suppressed.

4.5. Iris Filter

Kobatake et al. [48] adopted the iris filter to detect tumor candidates. This iris filter can enhance rounded convex regions such as tumors. It is so sensitive to tumors that the majorities of them give outputs larger than or equal to the seventh largest output in each mammogram. By this filtering, any tumor is expected and enhanced even if its contrast to its background is very weak.

This filter uses the orientation map of gradient vectors, which is similar to the method presented in [48]. However, definition and function of the iris filter are quite different. The idea of the iris filter is explained in a two-dimensional (2-D) continuous space. It is not applied to the image itself, but rather to its gradient vector field. The gradient vector at (x,y) is denoted by $g(x,y)$. It is obtained using the generation of gradients in two orthogonal directions. A Prewitt-type 3×3 operator is used for real digital mammograms. The region of support of the iris filter R_p is defined around the pixel P of interest. This is a combination of N half lines with a length R_{max} radiating from P . Q_i is an arbitrary pixel on the half line L_i . we define the convergence index of the gradient vector g at Q_i toward P as follows:

$$f(Q_i) = \cos \theta \text{ if } |g| \neq 0; f(Q_i) = 0 \text{ if } |g| = 0$$

where θ is the orientation of the gradient vector g at Q_i with respect to the i th half line. The convergence degree of gradient vectors on the line PQ_i , C_i , can be defined as the average of convergence indexes over the length PQ_i as follows

$$C_i = \left(\int_p^{Q_i} f(Q) dQ \right) / (\text{inverse of } (PQ_i))$$

The maximum convergence degree on the i th half line is $C_{io} = \max C_i$; $Q_i \in [P, R_i]$, where R_i is the most distant pixel from on the i th half line. The output of the iris

filter at the pixel of interest (x,y) is defined as average C_{io}

$$C(x,y) = 1/N \sum_{i=0}^{N-1} C_{io}$$

The output value of the iris filter $C(x,y)$ falls between -1 and 1. The point Q_i that maximizes the convergence degree is Q_{io} in the following. Its location depends on the distribution pattern of gradient vectors. Therefore, the size and shape of the substantial region of support of the iris filter changes for each location of P . Q_{io} can be considered a sample point of the boundary of the optimal 2-D region of support of the iris filter. The theoretical analysis of the iris filter shows that, if the gradient vector field is uniform, the iris filter shows a zero output.

4.6. Normalization of Local Contrast

The brightest pixels in a mammogram will often have a positive mean local value, because statistically these pixels have a high probability of being surrounded by darker pixels. This is especially true for pixels at small local peaks of the intensity distribution. In lower bins, the opposite effect occurs.

Veldkamp and Karssemeijer [133] presented an accurate adaptive approach for noise equalization. Here, the adaptive approach is optimized by investigating a number of alternative approaches to estimate the image noise. The estimation of high-frequency noise as a function of the grayscale is improved by a new technique for dividing the grayscale in sample intervals and by using a model for additive high-frequency noise. The adaptive noise equalization gives substantially better detection results than does fixed noise equalization. It is shown that relatively small adjustments in the algorithm have strong influence on the detection performance. Noise as a function of the gray level can then be obtained, and from this information, local contrast features are normalized.

4.7. Noise Equalization

McLoughlin et al. [72] extended a well-established film-screen noise equalization scheme for application to Full-Field Digital Mammogram (FFDM) images. A noise model is determined based on the assumption that quantum noise is dominant in direct digital X-ray imaging. Estimation of the noise as a function of the gray level is improved by calculating the noise statistics using a truncated distribution method. This square root model based approach, which FFDM allows, leads to a robust estimation of the high frequency image noise.

The use of a theoretical model for the dependency of noise variance on intensity in FFDM allows a straightforward and accurate approach to noise equalization. A consequence of excluding pixels near the breast edge from the noise estimation is that the maximum mean squared error found for the FFDM

images was slightly smaller than that found for the phantom images. The exclusions meant that the range of exposures for the FFDM images was less than for the phantom images; therefore, the range of exposures over which the error in the noise model fit was estimated was also less, making it easier to achieve a good fit.

4.8. Fractal Modeling

A fractal model has been used to describe the mammographic image, thus, allowing the use of a matched filtering stage to enhance microcalcifications against the background [8]. A region-growing algorithm, coupled with a neural classifier, detects existing lesions. Subsequently, a second fractal model is used to analyze their spatial arrangement so that the presence of microcalcification clusters can be detected and classified. In this model, the use of a FBM has permitted us to implement as optimized enhancement filter. Such a filter, along with ANN-based classifiers, exhibits good sensitivity and reasonable accuracy in detecting single microcalcifications, following a proper segmentation procedure. Microcalcification clustering has been modeled as fractal dust. In this way, it is able to extract effective descriptors of the spatial arrangements of microcalcifications. Fogel et al. [29] presented a linear discriminant models and artificial neural networks are trained to detect breast cancer in suspicious masses using radiographic features and patient age. The effectiveness of the classification procedures can be assessed using Receiver Operating Characteristic (ROC) analysis, where the probability of detecting a malignancy is traded off as a function of the likelihood of a false positive.

Li et al. [51] described a pattern-dependent enhancement algorithm based on fractal image modeling to analyze and model breast background structures. The general mammographic parenchymal and ductal patterns can be well modeled by a set of parameters of affine transformations. Therefore, microcalcifications can be enhanced by taking the judgment. It is found empirically that $\alpha = 3$ is a suitable choice. The final enhanced image $f_3(k,l)$ is

$$f_3(k,l) = f_2(k,l), \quad \text{if } f_2(k,l) \geq T; \quad 0, \quad \text{if } f_2(k,l) < T$$

It is showed that in terms of contrast, CII, PSNR, and ASNR, the fractal approach was the best, compared to the other methods. The noise level in the fractal approach was also lower than the other two methods.

4.9. Adaptive Density-weighted Contrast Enhancement

Patrick et al. [97] presented a approach for segmentation of suspicious mass regions in digitized mammograms using a new adaptive Density-Weighted Contrast Enhancement (DWCE) filter in conjunction with Laplacian-Gaussian (LG) edge detection. The DWCE enhances structures within the digitized mammogram so that a simple edge detection algorithm

difference between the original image and the modeled image. Reported results indicated that fractal models provide an adequate framework for medical image processing; consequently, high correct classification rates are achieved. A fractal modeling approach was used to analyze and model breast tissue background. Then, microcalcifications can be enhanced by employing the difference between the original image and the modeled image.

Microcalcifications can be enhanced by using the fractal modeling approach. Let $f(k,l)$ be the original image, and $g(k,l)$ be the modeled image after iterations. First, take the difference operation between $f(k,l)$ and $g(k,l)$ $f_1(k,l) = f(k,l) - g(k,l)$, $(k,l) \in N_1 \times N_2$ where $f_1(k,l)$ is the residue image. It is appropriate to ignore the negative value of the difference image $f_1(k,l)$. Because negative part of $f_1(k,l)$ does not contain any information about spots (including microcalcifications) brighter than the background, so, assume $f_2(k,l) = \max(0, f_1(k,l))$, $(k,l) \in N_1 \times N_2$ where $f_2(k,l)$ is the enhanced image from which background structures are removed. Image $f_2(k,l)$ contains useful signals and noises. Below a certain threshold T , any signal is considered unreliable. The threshold T is estimated from the image itself as α times the global standard deviation of the noise in an image $f_2(k,l)$. Thus, the value of α is the same for all images, but T depends on each individual image. T can be determined by a two-step estimation process.

First, the standard deviation of the whole image $f_2(k,l)$ is taken, and the initial threshold is chosen to be about 2.5 times this global standard deviation. Second, only those pixels in which the gray values are below the initial threshold are used to recalculate the standard deviation of the noise. This is a simplified version of a robust estimation of the standard deviation of noise. The final threshold T is determined by adjusting the value of α so that no subtle cases are missed using human

can be used to define the boundaries of the objects. Once the object boundaries are known, morphological features are extracted and used by a classification algorithm to differentiate regions within the image.

4.10. Modal-Based Image Enhancement

Highnam et al. [49] presented a way of estimating the scatter component of the signal at any pixel within a mammographic image, and use this estimate for model-based image enhancement. The first step is to divide breast tissue into "interesting" (fibrous/glandular/cancerous) tissue and fat. The scatter model is then based on the idea that the amount of scattered radiation reaching a point is related to the energy imparted to the surrounding neighborhood. This complex relationship is approximated using published empirical data and it varies with the size of the breast being imaged. The approximation takes the form of a

weighting mask which is convolved with the total signal (primary and scatter) to give a value which is input to a “scatter function”, approximated using three reference cases, and which returns a scatter estimate. Given a scatter estimate, the more important primary component can be calculated and used to create an image recognizable by a radiologist.

5. Segmentation

There are two different goals for the segmentation of microcalcifications [76]. One is to obtain the locations of suspicious areas to assist radiologists for diagnose. The other is to classify the abnormalities of the breast into benign or malignant. Local thresholding is used by setting threshold values for sub-images. It requires selection of a window size and threshold parameters. Wu et al. [140] presented that the threshold for a pixel is set as the mean value plus the Root Mean Square (RMS) noise value multiplied by a selected coefficient in a selected square region around the thresholded pixel [30,32]. Kallergi et al. [61] compared local thresholding and region growing

methods. It showed that the local thresholding method has greater stability, but is more dependent on parameter selection. Woods et al. [139] used local thresholding by subtracting the average intensity of a 15×15 window from the processed pixel. Then, region growing is performed

to group pixels into objects. Comparing with the multi-tolerance region growing algorithm [116, 69] and the active contour model, it showed that the speed of the algorithm is more than an order of magnitude faster than the other two.

Edge detection is a traditional method for segmentation. Many operators, Roberts gradient, Sobel gradient, Prewitt gradient and Laplacian operator, were published in the literature. Some mathematical morphological operations such as erosion, top-hat transformation and complicated morphological filters and multi-structure elements can also be used [56,57,93,100,150]. It is good in dealing with geometrically analytic aspects of image analysis problems. Stochastic approaches have also been used to

Table 2. An overview of Enhancement Techniques

Methods	Remarks
Modified median filter [117]	This filter can remove the noise without significantly distorting the signal.
Central Weighted Median Filter (CWWMF) [136].	A CWWMF with a large central weight preserves more image detail but suppresses less noise than a filter with a smaller central weight.
Model-based, scatter function [49]	A weighting mask has been calculated which represents the percentage of the total scatter reaching the central pixel and coming from the column of Lucite above each pixel in a neighborhood.
First derivative and the local statistics [68]	The adaptive image enhancement method exploits the first derivative operations using the Sobel operators, or the compass operators, and the local statistics of a mammographic image are used for an adaptive realization.
Fractal modeling [51]	The key point of fractal modeling is to explore the self-similarity property of images.
Fuzzy logic [9]	Has the potential of opening a new and promising direction for effective and early breast cancer diagnosis.
Wavelet transform, multiscale features [24]	Coherence measure and dominant orientation clearly improved discrimination of features from complex surrounding tissue and structure in dense mammograms.
Iris filter [48]	This filter output for the tumor is very high and its region is well isolated from its background.
Region-based Enhancement [43]	Region-based contrast enhancement uses each pixel as a seed to grow a region. Contrast is enhanced by applying an empirical transformation based on each region's seed pixel value, its contrast, and its background.
Wavelet, Morphological operation [25,110]	Fractal approach compared with the partial wavelet reconstruction and the morphological operation approaches.
Unsharp Masking, Sobel Operators [7,39]	The Unsharp masking method reduces the low frequency information while amplified the high frequency detail.
Adaptive noise equalization [133]	It gives much better results than does a fixed noise equalization, probably because noise characteristics are mammogram dependent, caused by variation of film type and film development characteristics.
Gaussian smoothing and sub sampling [94]	This method cumulatively modulate the intensity patterns of mass regions to form smooth hills with respect to their surroundings in the low-resolution image, and help in estimating the approximate extent of isolated regions present in the image.
Quantum noise assumption [72]	If quantum noise is assumed the dominant noise source present, a square root model will provide an accurate estimate of the noise with respect to gray level.
Matched filtering [8]	In particular, fractional Brownian motion (FBM) can model non-stationary random fields with stationary increments. In addition, a stationary power spectrum can be attached to FBMs leading to an approximate implementation of the enhancement filter via conventional matched filtering.

segment calcifications [62-65,133]. Stochastic and Bayesian methods have provided a general framework to model images and to express prior knowledge. Markov Random Field (MRF) model was used to deal with the spatial relations between the labels obtained in an iterative segmentation process [62-65]. The process-assigning pixel labels iteratively [25,98].

Fuzzy approaches: Apply fuzzy operators, property and inference rules to handle the uncertainty inherent in the image [10,21,22,103,104]. Region-based approach: Group pixel into homogeneous regions [116,135]. The fractal model: Image context can be modeled by fractal objects, which are attractors of sets of 2-D affine transformations [51,80]. Multiscale analysis: Design wavelet-based filters to transform the image from spatial domain to spatial frequency domain, and to perform further processing [143,144,121-126,136,96,22,38]. Statistical method: Using global or local statistics such as histogram, mean, standard deviation, etc [40,23].

5.1. Segmentation and Thresholding

Dengler et al. [57] presented systematic method for the detection and segmentation of microcalcifications in mammograms. This approach uses a two-stage algorithm for spot detection and shape extraction. The first stage applies a weighted difference of Gaussian filter for the noise-invariant and size specific detection of spots. A morphological filter reproduces the shape of the spots. In the detection process, the weighted difference of Gaussian makes use of the knowledge of the approximate size of the spots. It also requires an idea of the inter-spot distance. The precise knowledge of both sizes is not crucial, however. The basic idea is that the grey-value average within a spot. A simple way to measure the difference of these averages is a difference of Gaussian operation with a positive kernel of width $\sigma +$ reflecting the expected spot size, and a negative kernel of width $\sigma -$ reflecting the expected distance to neighboring spots.

Morphological filtering: The theory of mathematical morphology is powerful to analyze and describe geometrical relations. Essentially, it is a formalization of intuitive concepts such as size or shape. The two basic morphological operations are erosion and dilation, which are consistently defined for binary and gray value images. Let $B(x,y)$ be an image with $1 \leq x \leq n_1$ and $1 \leq y \leq n_2$ and M a structuring element representing a set of translations. As a structuring element, a disk with a diameter of 13 pixels was chosen. This is considered the maximal size of interest. In order to recover the positive peaks, the residual R of the opening is used: $R = B - (M \text{ OPENING } B)$

Here again the spots can be clearly seen, but obviously part of the noise remains. Therefore, a small threshold

has introduced in order to get rid of the noise. In order to reconstruct the shape of the spots optimally, both morphological and modified Difference of Gaussian (DOG) operator methods are combined. To control the image from growing beyond the original size, a morphological conditional thickening is applied. The results of both filters are combined with a conditional thickening operation. The topology and the number of the spots are determined with the first filter, and the shape by means of the second.

Kilday et al. [60] presented the classification of three common breast lesions, fibro adenomas, cysts, and cancers, was achieved using computerized image analysis of tumor shape in conjunction with patient age. The apparent method using all the features had the highest classification rate. The leaving-one-out test method using all the features resulted in a higher error rate than the two runs that used only a subset of the shape features. The increase in error rate using the leaving-one-out method is due to variability introduced into the classifier design in conjunction with the small number of samples.

5.2. Markov Random Field (MRF)

Li et al. [79] developed a technique for the detection of tumors in digital mammography. Detection is performed in two steps: segmentation and classification. The first step is choosing a prior interaction model, which was then tailor-fitted by a statistical method to the application of digital mammography. Initial segmentation scheme based on the knowledge, that suspicious areas are greatly brighter than their surrounding tissues. The first step is to separate the breast area from the background by simple thresholding. The threshold for this separation is selected from the peak of the average contrast histogram. In multi resolution segmentation, pixel classification is performed by progressively segmenting an image from coarse (low) to fine (high) spatial resolution. The segmentation is improved and small windows give more reliable and accurate estimates.

In classification of extracted regions, the selected features should have the characteristics like, discrimination, reliability, independence and small number. Moreover, the fuzzy binary decision tree procedure contains three steps: 1) splitting nodes, 2) determining terminal nodes, and 3) assigning a class to the terminal nodes. In this method, the training data set is split into two independent sets. A large tree is grown based on the first training set by splitting until all terminal nodes have pure class membership. Then a pruned sub tree is selected by minimizing the second training

Table. 3 An Overview of Segmentation

Methods	Remarks
Gaussian filter, morphological filter, conditional thickening [57]	The weighted difference of Gaussian makes use of the knowledge of the approximate size of the spots. It also requires an idea of the inter-spot distance. The precise knowledge of both sizes is not crucial, however. The basic idea is that the grey-value average within a spot.
Adaptive thresholding, MRF model-based method, fuzzy binary decision tree [79]	An MRF model-based segmentation belongs to partitional clustering, but it also has the ability to model image joint distributions in terms of local spatial interaction.
Fractal model [51,76,80]	Mammograms possess structures with high local self-similarity that is the basic property of fractal object. However, the computation time is high.
Region growing approach, Surrounding region dependence [56,69,116,135]	Works best when the region homogeneity criterion is easy to define. It depends on the selection of seed region and the termination conditions. It is expensive in both computational time and memory.
Top-hat, Morphological filter with multiscale and Multi elements, Erosion [56,57,100,150,93]	When using the multiscale and multi-structuring elements, the results are not affected by the complex background and the extracted images are not distorted much. However, it requires a priori knowledge of the resolution level of the mammograms in order to determine the sizes and shapes of the structure elements.
Histogram thresholding, MRF [30,32,40,61-64,76,93,101, 116, 126,133,139,140,]	It does not need a prior information for the histogram thresholding of the image and can be used widely work very well with low computation complexity, but it do not work without peaks and sometimes the segmented region cannot be contiguous.
Fuzzy logic [103,10,22,23,104]	Due to variable shapes of microcalcifications, it is a good way to use fuzzy rules to perform approximate inference. However, the determination of fuzzy membership is not easy.
Multichannel wavelet transform, Multiscale analysis, Decimated wavelet transform [10,21,38,95,96,104,120,122-126,136,143,144]	Due to its ability of discriminating different frequencies, the method can preserve the resolution of the portion of ROI. Moreover, it does not require the use of heuristics or a prior knowledge of the size and the resolution of the mammogram.
Edge detection, thresholding, Deformable model [44]	A partial Thresholding is performed for noise reduction. A setting threshold value is also obtained from the edge detector evaluation. This image is introduced as input to the local approach stage, where the contour snake is initialized with a circumference.
Straight line estimation and iterative cliff detection [128]	Straight-line estimation is carried out within a region of interest (ROI). The straight line is then tested for validity. If valid, the ROI is adjusted accordingly, and a second straight-line estimation is performed in the new ROI. If the second straight line is also valid, it is used as the input to iterative cliff detection.

set estimate of the misclassification rate over all the pruned sub trees. The procedure is then iterated, successively interchanging the roles of the first and second training sets.

5.3. Deformable Models

Valverde et al. [44] presented an algorithm for the segmentation of vessels in mammograms, which is very useful for the elimination of vascular false positives during detection of microcalcification in mammograms. The main problem is the high level of noise presence in mammograms. Two approaches (stages) have been used to deal with this problem. First, a theoretical analysis of edge detection is carried out in order to select the optimum edge detector and threshold value. This is applied to the whole image to improve the Signal to Noise (S/N) ratio thus avoiding significant signal loss. Second, a local approach, where local noise - represented as particle noise, remaining in the image from the global noise reduction - is removed by a

segmentation process based on a snake with a new noise energy term, which extracts the vessel contour.

6. Microcalcification Detection

In this section, a few most important and efficient techniques for microcalcification detection are studied and compared.

6.1. Wavelet

Bruce et al. [81] applied the discrete wavelet transform mod-max method, to the problem of mammographic mass classification. This method was used to extract multiresolution features that quantify the mass shapes. Three new features were developed: variation ratio mean, variation ratio standard deviation, and the Lipschitz sum. These features were compared with traditional uniresolutional shape features in their ability to discriminate between shape classes. These features provided a means of evaluating the shapes at various scales. When utilizing a statistical classification system with Euclidean distance measures determining

class membership, the use of multiresolution features significantly increased the classification rates.

Ferrari et al. [41] presented a new method for the identification of the pectoral muscle in MLO mammograms based upon a multiresolution technique using Gabor wavelets. This new method overcomes the limitation of the straight-line representation considered in initial investigation using the Hough transform. The method starts by convolving a group of Gabor filters, specially designed for enhancing the pectoral muscle edge, with the region of interest containing the pectoral muscle. After computing the magnitude and phase images using a vector-summation procedure, the magnitude value of each pixel is propagated in the direction of the phase. The resulting image is then used to detect the relevant edges. Finally, a post-processing stage is used to find the true pectoral muscle edge.

Chun-Ming Chang et al. [24] developed an enhancement algorithm relying on multiscale wavelet analysis and extracted oriented information at each scale of analysis was investigated. The evolution of wavelet coefficients across scales characterized well the local shape of irregular structures. Using oriented information to detect features of an image appears to be a promising approach for enhancing complex structures and subtle tissues of the breast. Steerable filters that can be rotated at arbitrary orientations reliably found visual cues within each spatial frequency sub-band of an image. Coherence measure and dominant orientation clearly improved discrimination of features from complex surrounding tissue and structure in dense mammograms.

Wavelet theory provides a powerful framework for multiresolution analysis, and it can be used for texture analysis. The discrete wavelet transform is used to map the ROIs into a series of coefficients, which constituted a multiscale representation of the ROIs. To obtain the features reflecting scale-dependent properties, a set of features can be extracted from each scale of the wavelet transform. The most frequently used features are energy, entropy, and norm of the coefficients [37,67,108,122,145,146].

Lemaur et al. [78] provided new wavelets with a higher Sobolev regularity compared with the classical wavelets, assuming the same support width. Contrary to the classical smoothness or moment regularity of a wavelet (null moment's property), the Sobolev regularity refers to the fractional derivatives of the signal (image) and to its singular spectrum, says a more sophisticated structure.

6.1.1. New Wavelets

To construct new compactly supported wavelets, let $Q_{N,K}(x)$ a polynomial of degree $2N + 2K - 1$ (N, K are non null positive integers) such that $Q_{N,K}(x) = \varepsilon_{N,K} \int_{-1}^x (1-t^2)^{N-1} P_K(t^2) dt$ (4)

where $\varepsilon_{N,K}$ is set such that $Q_{N,K}(1) = 1$ and $P_K(t^2)$ is any polynomial of degree K such that $Q_{N,K}(x) \geq 0$. Clearly, $Q_{N,K}$ fulfills the conditions cited to construct wavelets with the polynomial $Q_{N,K}(x)$. However, to use $Q_{N,K}(x)$ for the construction of compactly supported wavelets, one must first verify that $Q_{N,K}(x)$ is positive on $[0,1]$ and does not vanish on $[1/2,1]$. Note that the wavelet issued from $Q_{N,K}(x)$ will have N null moments and that its support width is $\Omega_{N,K} = 2N + 2K - 1$.

There exists an interesting family of polynomials called the Matzinger polynomials, which leads to wavelets with an improved regularity index. To obtain such wavelets have to replace, in formula (4), $P_K(t^2)$ by

$$(1 - \alpha^2 t^2)^{2K-1} (1 - \beta^2 t^2) \text{ which yields} \\ Q_{N,2K}(x) = \varepsilon_{N,2K} \int_{-1}^x (1-t^2)^{N-1} (1-\alpha^2 t^2)^{2K-1} (1-\beta^2 t^2) dt \quad (5)$$

where α is chosen such that $1 < \alpha \leq 2$ and $\varepsilon_{N,2K}$ such that $Q_{N,2K}(1) = 1$.

One needs to set $Q_{N,2K}(1-\alpha) = 0$ to let $Q_{N,2K}(x)$ verify the non-vanishing condition cited above. According to the variations of $Q_{N,2K}$, to compute β , have to solve the following equation:

$$\int_{-1}^{-1/\alpha} (1-t^2)^{N-1} (1 - \alpha^2 t^2)^{2K-1} (1-\beta^2 t^2) dt = 0.$$

One gets β , $1 < \beta < \alpha$. In this case $P_K(t^2)$, has roots $\{\pm 1/\alpha, \pm 1/\beta\}$ lying in the unit circle. For more details about this humdrum calculus, also show that $Q_{N,2K}(x)$ verifies all the conditions as soon as the inequality $0 < 2K \leq N$. (in eq. (6) or in eq. (4) is satisfied)

6.1.2. Regularity Ratio Estimates for the New Wavelets

In this section, show that using the new family of wavelets introduced above in formula (5), new wavelets can construct which have a higher regularity ratio than the Daubechies ones for the same support width. Denote by the Sobolev regularity of the new wavelet. Since $Q_{L,K}(x)$ has roots at -1 , here L denotes a non-null integer, and one gets (6).

$Q_{L,K}(x) = [((1+x)/2)]^L A(x)$. where $A(x)$ is a polynomial of degree $L + 2K + 1$. To compute the regularity ratio of the new wavelets, use a classical result. Let the equation shown at the bottom of the page hold then have for the Holder regularity, denoted here by σ'

$$L - (1/2 \ln 2) \ln \rho_1 \leq \sigma' \leq L - (1/2 \ln 2) \ln \rho_2 \quad (6)$$

Moreover, the same result states also that, having,

$$\sigma' - 1/2 \leq \sigma \leq \sigma' \quad (7)$$

6.2. Wavelet Expansion

Heine et al. [58] developed a method for identifying clinically normal tissue in digitized mammograms is used to construct an algorithm for separating normal regions from potentially abnormal regions; i.e., small regions that may contain isolated calcifications. The first step is to decompose the image with a wavelet expansion that yields a sum of

independent images, each containing different levels of image detail. When calcifications are present, there is strong empirical evidence that only some of the image components are necessary for detecting a deviation from normal. The underlying statistic for each of the selected expansion components can be modeled with a simple parametric probability distribution function. This function serves as an instrument for the development of a statistical test that allows for the recognition of normal tissue regions. The distribution function depends on only one parameter, and this parameter itself has an underlying statistical distribution. The values of this parameter define a summary statistic that can be used to set detection error rates. Once the summary statistic is determined, spatial filters that are matched to resolution are applied independently to each selected expansion image. Regions of the image that correlate with the normal statistical model are discarded and regions in disagreement (suspicious areas) are flagged. These results are combined to produce a detection output image consisting only of suspicious areas. This type of detection output is amenable to further processing that may ultimately lead to a fully automated algorithm for the identification of normal mammograms.

6.3. Wavelet Based Sub band Decomposition

Wand and Karayiannis [129] presented an approach for detecting microcalcifications in digital mammograms employing wavelet-based sub-band image decomposition. The microcalcifications appear in small clusters of few pixels with relatively high intensity compared with their neighboring pixels. These image features can be preserved by a detection system that employs a suitable image transform which can localize the signal characteristics in the original and the transform domain. Given that the microcalcifications correspond to high-frequency components of the image spectrum, detection of microcalcifications is achieved by decomposing the mammograms into different frequency sub-bands, suppressing the low-frequency sub-band, and, finally, reconstructing the mammogram from the sub-bands containing only high frequencies.

Strickland et al. [126] developed a two-stage method based on wavelet transforms for detecting and segmenting calcifications. The first stage is based on an Undecimated wavelet transform, which is simple than the conventional filter bank implementation without down sampling, so that the low-low (LL), low-high (LH), high-low (HL), and high-high (HH) sub-bands remain at full size. The second stage is designed to overcome the limitations of the simplistic Gaussian assumption and provides an accurate segmentation of calcification boundaries. Detected pixel sites in HH and LH+HL are dilated then weighted before computing the inverse wavelet transform. Individual microcalcifications are greatly enhanced in the output image, to the point where straightforward thresholding

can be applied to segment them. Free-response Receiver Operating Characteristic (FROC) curves are computed from tests using a freely distributed database of digitized mammograms. By combining sub-bands from the multiple transforms, it is conceivable that background structures could be favorably suppressed.

6.4. Shape Features Wavelet

Dhawan et al. [37] presented a gray-level image structure feature based approach for the analysis and classification of “difficult-to-diagnose” mammographic microcalcifications. The combined set of image structure included features from second order gray-level histogram statistics for representing global texture and wavelet decomposition-bases features for representing local texture of the microcalcifications area of interest, and first-order gray-level features from the segmented microcalcification regions.

6.5. Template Matching

Lai et al. [117] presented a method for detecting one type of breast tumor, circumscribed masses, in mammograms. It relies on a combination of criteria used by experts including the shape, brightness contrast, and uniform density of tumor areas. In the first step, median filtering is used to enhance mammogram images and template matching to detect breast tumors. The second step is concerned with tumor detection. This method is based on template matching and is capable of detecting suspicious areas in mammograms independent of their size, orientation, and position.

Leung et al. [118] presented a method for the mammographic detection and classification of two types of breast tumors, stellate lesions and circumscribed lesions. The method assumes that both types of tumors appear as approximately circular, bright masses with a fuzzy boundary and that stellate lesions are in addition surrounded by a radiating structure of sharp, fine lines.

6.6. Feature Extraction

Mudigonda et al. [94] developed a method for the detection of masses in mammographic images. Features based on flow orientation in adaptive ribbons of pixels across the margins of masses are used to classify the regions detected as true mass regions or False-Positives (FPs). The mass regions that were successfully segmented were further classified as benign or malignant disease by computing five texture features based on Gray-level Co-occurrence Matrices (GCMs) and using the features in a logistic regression method. The features were computed using adaptive ribbons of pixels across the boundaries of the masses.

Karssemeijer and Veldkamp [65] also use a large set of microcalcification Features, form a feature vector, and their distributions are used as cluster features. In the first stage, Zhang et al. [149] used a set of microcalcification features as the inputs of a back-propagation neural network to reduce the false detection. In the second Davies et al. [31] used fewer

features: area, mean gray level, ratio of area to the square of the maximum linear dimension, shape parameter, and edge strength.

Gulsrud et al. [131] dealt with the problem of texture feature extraction in digital mammograms. The feature extraction scheme contains two filters, the optimal filter and the smoothing filter. This filter combination should be designed in such a way that the classification of the feature images becomes as successful as possible. In the design process, both the filter coefficients and the filter size and shape have to be determined. Concerning the shape of the filters, due to the relatively random shapes and orientations of microcalcifications, it is not possible to find a filter shape that matches each different microcalcification. Thus, for simplicity, choose to only consider filters with a square support. Starting with the optimal filter, finding corresponding smoothing filter should be relatively small. The results indicate that the optimal filter-based method is very well suited for automated detection of clustered microcalcifications.

Verma and Zakos [134] presented a system based on fuzzy-neural and feature extraction techniques for detecting and diagnosing microcalcifications' patterns in digital mammograms. A combination of three features, such as entropy, standard deviation, and number of pixels, is the best combination to distinguish a benign microcalcification pattern from one that is malignant is used. A fuzzy technique in conjunction with three features was used to detect a microcalcification pattern and a neural network to classify it into benign/malignant.

The fuzzy detection algorithm aims at detecting micro calcifications and suspicious areas. It uses a 16×16 window to scan over the entire digital mammogram and locate Microcalcification or other abnormalities: The algorithm only detects the center pixel of a microcalcification area. It is up to the user to view the surrounding area to decide how big the microcalcification area actually is. Microcalcification areas vary greatly in size, shape, and grey color. Therefore, it is very difficult to develop a good algorithm that is effective at detecting microcalcifications based only on digital image processing and FL.

The most significant feature or combination of features was selected based on neural-network classification. It was done by starting with a single feature by feeding it to the neural network and analyzing the classification rate. If it was increased or unchanged by adding a particular feature, then include this feature to the input vector. Otherwise, remove this feature, added another feature to the existing input vector, and repeated the whole process again.

Matsubara et al. [85] (Binarization Technique) developed two detection approaches for architectural

distortions existing around skinline and within mammary glandular tissues.

6.7. Fuzzy Logic and Scale Space Techniques

Netsch and Peitgen [96] described a method for the automated detection of microcalcifications in digitized mammograms. The method is based on the Laplacian scale-space representation of the mammogram only. First, possible locations of microcalcifications are identified as local maxima in the filtered image on a range of scales. For each finding, the size and local contrast is estimated, based on the Laplacian response denoted as the scale-space signature. A finding is marked as a microcalcification if the estimated contrast is larger than a predefined threshold, which depends on the size of the finding. It is shown that the signature has a characteristic peak, revealing the corresponding image features. This peak can be robustly determined. The basic method is significantly improved by consideration of the statistical variation of the estimated contrast, which is the result of the complex noise characteristic of the mammograms. The method is evaluated with the Nijmegen database and compared to other methods using these mammograms. Results are presented as the FROC performance. At a rate of one false positive cluster per image, the method reaches a sensitivity of 0.84, which is comparable to the best results achieved.

H.D. Cheng et al. [19] presented a novel approach to microcalcification detection based on fuzzy logic and scale space techniques. First, the fuzzy entropy principal and fuzzy set theory is used to fuzzify the images. Then, enhance the fuzzified image. Finally, scale-space and Laplacian-of-Gaussian filter techniques are used to detect the sizes and locations of microcalcifications. A free-response operating characteristic curve is used to evaluate the performance. The major advantage of the method is its ability to detect microcalcifications even in the mammograms of very dense breasts. Experimental results demonstrate that the microcalcifications can be accurately detected.

6.7.1. Normalization and Fuzzification

The mammograms have different brightness and contrast due to the varying illumination. In order to reduce the variation and achieve computational consistency, the images are normalized. Map all the mammograms into a fixed intensities range r_1 and r_2 ($0 \leq r_1 < r_2 \leq 255$). Assume an image $g_i(x,y)$ whose maximum gray level is $\max G_i$ and minimum gray level is $\min G_i$ and transform $g_i(x,y)$ into $G_k(x,y)$

$$G_k(x,y) = r_1 + [(g_i(x,y) - \min G_i) \times (r_2 - r_1)] / [\max G_i - \min G_i]$$

In this experiment, choose $r_1 = 60$ and $r_2 = 210$ due to the fact that maximum intensities and minimum intensities of the microcalcifications are not beyond r_2 and below r_1 with certainty after investigating a huge amount of mammograms. Mammograms have some degree of fuzziness such as indistinct borders, ill-

defined shapes and different densities. Mammographic enhancement is essential and important for reducing both the FN and FP rates. Homogeneity is mainly related to the local information of an image and reflects how uniform an image region is. A method is adopted for enhancing the mammograms that uses both global and local information. The Laplacian-of-a-Gaussian ($\nabla^2 G$) filter has been applied to variety tasks in multi-scale image analysis, such as region detection and contrast enhancement. Gaussian smoothing has the effects: simplification by removing the fine scale features and distortion by flattening, dislocating and broadening of the surviving features.

Fuzzy theory and scale space is used to automatically detect microcalcification clusters in

6.8. Statistical Analysis

Karssemeijer [98] described a method to detect such stellate patterns. This method is based on statistical analysis of a map of pixel orientations. An important feature of the method is that the way in which an orientation of the image intensity map is determined at each pixel. A new method, based on the application of second-order operators, is presented for this purpose. If a line-like structure is present at a given site, the method provides an estimate of the orientation of this structure, whereas in other cases the image noise will generate a random orientation. Using scale space theory it will be shown how accurate estimates of line orientation can be obtained at a given scale from the output of only the directional, second-order, Gaussian derivative operators, differing by $\pi/3$ in orientation.

The line-based orientation estimates are used to construct two operators that respond to radial patterns of straight lines. Combination of the output of these operators in a classifier leads to a very sensitive method for detection of stellate patterns. The method is applied to detect stellate lesions and architectural distortion in mammograms from MIAS database.

Another issue, which is investigated in here, is application of k-nearest neighbor, a neural network, and a decision tree for classification. In addition, the use of multiple scales for estimation of line orientation is validated by determining the performance at different single spatial scales. The results show that based on a line-based pixel orientation map many subtle spiculated lesions and architectural distortions can be detected at a high degree of specificity.

6.8.1. Gray Level Image Texture Feature

Dhawan et al. [37] defined a set of image structure features for classification or malignancy. Two categories of correlated gray-level image structure features are defined for classification of “difficult-to-diagnose” cases. Surrounding Region Dependence Method (SRDM) is based on a second order histogram

digitized mammograms. This approach is very efficient and effective for locating microcalcifications in the mammograms with various densities. (1) The micro calcifications can be accurately detected even in mammograms of very dense breast. (2) Mammogram enhancement is more adaptive and robust. (3) definition of the contrast based on fuzzy homogeneity uses both local and global information and the contrast enhancement algorithm can enhance the main feature while suppress the noise. (4) the parameters can be easily adjusted to obtain different True-Positives (TP) and False-Positives (FP) rates that are useful for deriving ROC or FROC curves. (5) Threshold factor is determined by neural network considering statistical and fuzzy nature of the mammograms.

matrix that is calculated from two surrounding regions of a pixel [67,75]. The textural features can be extracted from the co-occurrence matrix. They are related to specific textural characteristics such as the homogeneity, contrast, entropy, energy and regularity of the structure within the image [27,36,37,39,43,86]. Pettazzoni et al. [107] provided a general scheme for detection and/or automated recognition of microcalcifications. Some modules that perform ROI selection is introduced, using special non-linear filters designed for microcalcification detection.

6.9. Non-Linear Filtering

A first type of filter selects pixels with specific statistical local features, as compared to the local mean. Among these, only pixels satisfying particular constraints on the local standard deviation are kept. Another type of filter then checks the local mean values of gradient components, so that sharp variations, unrelated to small close objects, can be eliminated. The scheme thus applies different non-linear filters in combination, making precise identification of clustered microcalcifications possible. This modular approach seems greatly to simplify system maintenance and consistency, as well as affording a comparison of different processing techniques and parameters.

Bhangale et al. [7] and Rogova et al. [110] used a set of Gabor filters to process mammograms. By changing the center frequencies of Gabor filters, this method could change the original images into different scales and orientation spaces. Fractal dimension is a numerical value used to characterize a fractal, and it can be used as an indicator of the roughness of an image. Smoother areas of the images have lower fractal dimension values than rougher areas [12,39,110].

Hojjatoleslami and Kittler [50] used the number of microcalcifications within a region of a fixed area. A square of 1 cm^2 is used as discontinuity measure to distinguish a new cluster. Nishikawa et al. [102] used the similar technology with [50] the features extracted from mammogram directly such as perimeter, area, compactness, elongation, eccentricity, thickness,

orientation, direction, line, background, foreground, distance, and contrast. They are easy to extract and they originate from the experience of radiologists. Features used to describe the distribution of the microcalcification. [10,30,18,64,65,83,95,99-101,115,138,139,145], cluster area, and number of microcalcifications in an area [16,25,102].

6.10. Adaptive Thresholding

Hatanka et al. [147] devised an adaptive thresholding technique for detecting masses. The partial loss masses are identified by their similarity to a sector-form model in the template matching process.

Table 4. An Overview of Detection of Microcalcifications

Methods	Remarks
Median filter, template matching [117]	A coarse-fine template matching method was implemented, and the results show that the computational cost can be reduced.
Edge-oriented approach, field-oriented approach, spine-oriented approach [118]	Assumes that both types of tumors appear as approximately circular, bright masses with a fuzzy boundary and that stellate lesions are in addition surrounded by a radiating structure of sharp, fine lines.
Gaussian derivative operators [98]	A new method, based on the application of second-order operators, is presented here.
Undecimated wavelet transform [126]	By combining sub-bands from the multiple transforms, it is conceivable that background structures could be favorably suppressed.
Wavelet decomposition, multivariate cluster analysis, GA-based global search method [37]	The combined set of image structure included features from second order gray-level histogram statistics for representing global texture and wavelet decomposition-bases features for representing local texture of the microcalcifications area of interest, and first-order gray-level features from the segmented microcalcification regions.
Wavelet expansion, parametric probability distribution function [58]	Used to construct an algorithm for separating normal regions from potentially abnormal regions; that is, small regions that may contain isolated calcifications.
Wavelet-based sub-band image decomposition [129]	The microcalcifications appear in small clusters of few pixels with relatively high intensity compared with their neighboring pixels.
Discrete wavelet transform mod-max method [81]	This method was used to extract multiresolutional features that quantify the mass shapes.
Laplacian scale-space representation [96]	A finding is marked as a microcalcification if the estimated contrast is larger than a predefined threshold, which depends on the size of the finding.
Multiscale wavelet analysis [24]	The discrete wavelet transform is used to map the ROIs into a series of coefficients, which constituted a multiscale representation of the ROIs.
Fuzzy-genetic approach [13]	This system first attains high classification performance with the possibility of attributing a confidence measure to the output diagnosis; second, the resulting systems involve a few simple rules.
Scale-space features [96]	Features extracted from the image processed by Laplacian of Gaussian filter.
Fractal dimension [14,103,110]	Features extracted from fractal model of the image
Gray level run length (GLRL) Features [67]	Features extracted from the GLRL matrix
Surround region dependence (SRDM) features [67,75]	Four directional-weighted sum extracted from the SRDM
Gray Level Difference (GLD) Features [67]	Features extracted from the GLD matrix
Wavelet features [37,122,68]	Energy, entropy, and norm extracted from the wavelet transform sub-images
Gabor filter bank features [7,110]	Features extracted from Gabor filter bank processed image
Co-occurrence features [27,37,39,87,43,145]	Features extracted from spatial gray level dependence matrix (co-occurrence matrix)
Texture features, gray-level co-occurrence features [27,37,39,87,43,145]	A pyramidal representation of the given image is obtained by iterative decimation operations on the full-resolution image, thereby generating a hierarchy of sub images with progressively decreasing bandwidth and increasing scale.
Co-occurrence Features [27,37,39,43,86,145]	Starting with the optimal filter, finding corresponding smoothing filter should be relatively small.
Fuzzy-neural and feature extraction techniques, BPNN [11]	A fuzzy technique in conjunction with three features was used to detect a microcalcification pattern and a neural network to classify it into benign/malignant.
Non-linear filters [107]	It seems greatly to simplify system maintenance and consistency, as well as affording a comparison of different processing techniques.
Adaptive thresholding [147]	The partial loss masses are identified by their similarity to a sector-form model in the template matching process.
Individual features of microcalcification [5,10,18,31,64,84,85,99,100,115,138,145,149,139]	Features extracted from mammogram directly such as perimeter, area, compactness, thickness, direction, line, background, foreground, distance and contrast. They are easy to extract and they originate from the experience of radiologists.
Individual features of microcalcifications [5,10,18,31,54,83,84,99,100,115,138,139,145,149]	Features used to describe the distribution of the microcalcification, cluster area, and number of microcalcifications in an area.
Contrast features, Sobolev regularity [78]	Two detection approaches for architectural distortions existing around skinline and within mammary glandular tissues
Binarization technique, top-hat process [85]	Contrary to the classical smoothness or moment regularity of a wavelet, the Sobolev regularity refers to the fractional derivatives of the signal (image) and to its singular spectrum, says a more sophisticated structure.
Radial density profile, template matching, and Correlation Matching [82]	After computing the magnitude and phase images using a vector-summation procedure, the magnitude value of each pixel is propagated in the direction of the phase. The resulting image is then used to detect the relevant edges.
Fuzzy set theory, scale-space and LOG filter [19]	Radial density profiles can be used to describe and compare radial mass distribution in any circular, spherical or cylindrical shape.
	The major advantage of this method is its ability to detect microcalcifications even in the mammograms of very dense breasts.

To calculate the similarity, four features are applied: 1) average pixel value; 2) standard deviation of pixel values; 3) standard correlation coefficient defined by the sector-form model; and 4) concentration feature determined from the density gradient. The FPs were eliminated using a second-order statistics technique. There were four parameters utilized. From the gray-level co-occurrence matrix, three second-order statistics values, angular second moment (ASM), inverse difference moment (IDM), and entropy (ENT), were calculated. In addition, a contrast (CNT) was set by the matrix based on the gray-level difference method.

6.11. Fuzzy – Genetic

Andres et al. [13] applied a combined fuzzy-genetic approach to the Wisconsin breast cancer diagnosis problem. These evolved systems first attain high classification performance with the possibility of attributing a confidence measure to the output diagnosis; second, the resulting systems involve a few simple rules, and are therefore interpretable. The fuzzy-genetic approach is highly effective where such medical diagnosis problems are concerned.

7. Classifiers

Some of the classifiers are studied and compared in the following sections.

7.1. Artificial Neural Network

L. Zheng and Chan [77] described an algorithm that acts as a preprocessor for marking out suspicious tumor regions in a mammogram. Discrete Wavelet Transform (DWT)-based Multiresolution Markov Random Field (MMRF) segmentation is used for segmentation. In the procedure an image is first decomposed using DWT and the segmentation starts from the LL sub band of the coarsest resolution level. To avoid over-smoothing at this level, LL sub band image size is restricted to be at least 128×128 . The MRF segmentation results are propagated according to the self-similarity mapping relations between different levels until to the finest level. In this application, the Iterated Conditional Modes (ICM) is chosen to find the Maximum a Posterior (MAP) estimation for the MRF because of its high efficient performance. After the segmentation procedure, the analyzed mammogram will be segmented into different regions according to their gray-levels and texture. The features of each region will be generated in the classification step for tumor detection. All feature parameters of a given extracted region are input into the binary decision tree. Each node in this tree contains a threshold for the feature it represents and the input data will flow along the direction of the arrows based on the result at each node. When the signal reaches the end, a classification result has been made. The following figure shows the block diagram of a typical classification scheme.

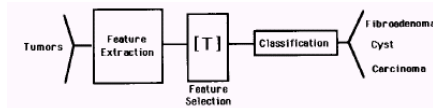


Figure 7.1 Block Diagram of a typical Classification Scheme

Rudy Setiono [112] described how the accuracy of the networks and the accuracy of the rules extracted from them could be improved by a simple pre-processing of the data. Data pre-processing involves selecting the relevant input attributes and removing those samples with missing attribute values. The rules generated by neural network rule extraction algorithm are more concise and accurate than those generated by other rule generating methods reported in the literature. The outline of the rule extraction method is as follows, (1) Select and trains a network to meet the pre specified accuracy requirement. (2) Remove the redundant connections in the network by pruning while maintaining its accuracy. (3) Discretize the hidden unit activation values of the pruned network by clustering. (4) Extract rules that describe the network outputs in terms of the discretized hidden unit activation values. (5) Generate the rules that describe the discretized hidden unit activation values in terms of the network inputs. (6) Merge the two sets of rules generated in steps 4 and 5 to obtain a set of rules that relates the inputs and outputs of the network.

Bocchi et al. [8] described a method to detect microcalcifications from standard mammograms. The Fractional Brownian Motion (FBM) has permitted us to implement an optimized enhancement filter. Such a filter, along with ANN-based classifiers, exhibits good sensitivity and reasonable accuracy in detecting single microcalcifications. Following a proper segmentation procedure, microcalcification clustering has been modeled as fractal dust. In this way, it is able to extract effective descriptors of the spatial arrangements of microcalcifications. It must be pointed out that conventional FBMs can be extended in several directions to reflect, even more closely, the complexity of the imaged anatomy. Thus, the use of a space varying Hurst's exponent is plausible. This method based mainly on the size and contrast of μCa spots. This would allow higher detection accuracy, the shape of microcalcifications is diagnostically relevant and can be used to evaluate their possible degree of malignancy.

An artificial neural network is a parallel, distributed information processing structure consisting of processing elements interconnected by directional connections. A neural element carries out local operations. Distinct classes: suspicious and probably benign. An optimal neural network architecture selected by a simulated annealing optimization technique was used to improve the classification performance [71,36,55,70,75, 134,11, 138]. Genetic algorithms were

also used to optimize the features for differentiating malignant from benign [3,114,15].

K-nearest neighbor (KNN) classifier distinguishes unknown patterns based on the similarity to known samples. The KNN algorithm computes the distances from an unknown pattern to every sample and selects the K nearest samples as the base for classification. The unknown pattern is assigned to the class containing the most samples among the K-nearest samples [26,71,148].

7.2. Pattern Recognition Algorithm

Disagreement or inconsistencies in mammographic interpretation motivate utilizing computerized pattern recognition algorithms to aid the assessment of radiographic features. Fogel et al. (1998a) have studied the potential for using Artificial Neural Networks (ANNs) to analyze interpreted radiographic features from film screen mammograms. For suspicious masses, the best-evolved ANNs generates a mean area under the receiver operating characteristic curve (A_z) of 0.9196 ± 0.0040 , with a mean specificity of 0.6269 ± 0.0272 at 0.95 sensitivity. Results when microcalcifications were included were not quite as good ($A_z = 0.8464$), however, ANNs with only two hidden nodes performed as well as more complex ANNs and better than ANNs with only one hidden node. The success of small ANNs in diagnosing breast cancer offers the promise that suitable explanation for the ANN's behavior can be induced, leading to a greater acceptance by physicians.

Bayesian Belief Network (BBN) is an optimal pattern recognition method; it uses a probabilistic approach to determine an optimal segmentation given a specific database [139,151,79]. Binary decision tree is an ordered list of binary threshold operations on the features organized as a tree. Each node will move down to its two descendents by thresholding values of the features. This procedure will continue until it arrives at a terminal node, which assigns a classification [77].

7.3. Adaptive Resonance Theory

Kim et al. [68] designed a new type of classifier combining an unsupervised and a supervised model and applied to classification of malignant and benign masses on mammograms. The unsupervised model was based on an Adaptive Resonance Theory (ART2) network that clustered the masses into a number of separate classes. The classes were divided into two types: one containing only malignant masses and the other containing a mix of malignant and benign masses. The masses from the malignant classes were classified by ART2. The masses from the mixed classes were input to a supervised Linear Discriminant Classifier (LDA). In this way, some malignant masses were separated and classified by ART2 and the less distinguishable benign and malignant masses were classified by LDA. Receiver operating Characteristics

analysis was used to evaluate the accuracy of the classifiers. The average area under the ROC curve (A_z) for the hybrid classifier was 0.81 as compared to 0.78 for the LDA and 0.80 for the BPN. The partial areas above a true positive fraction of 0.9 were 0.34, 0.27 and 0.31 for the hybrid, the LDA and the BPN classifier, respectively. These results indicated that the hybrid classifier is a promising approach for improving the accuracy of classification in CAD applications.

7.4. Hybrid Neural Network Classification

Papadopoulou et al. [106] presented a hybrid intelligent system for the identification of microcalcification clusters in digital mammograms. The hybrid intelligent system employs two components: a rule based and a neural network sub-system. The rule construction procedure consists of the feature identification step as well as the selection of the particular threshold value for each feature. First, visualization of all the calculated features in two-dimensional plots, in pairs, has been employed for the selection of suitable feature threshold values that lead to the categorization of a remarkable number of ROIs. For every feature, several threshold values are examined in the range of values corresponding to that feature. For each threshold value, the number of ROIs below and above the threshold value is recorded. The ratio of the number of ROIs that belong to a specific class (normal or pathological) over the total number of the ROIs that belong to the same class should be more than 6%. In addition, the number of the false negative ROIs must be equal or less than one.

Lim et al. [17] presented a study of the application of autonomously learning multiple neural network systems to medical pattern classification tasks. The hybrid neural network architecture has been developed for on-line learning and probability estimation tasks. The network has been shown to be capable of asymptotically achieving the Bayes optimal classification rates, on-line, in a number of benchmark classification experiments. In the context of pattern classification, however, the concept of multiple classifier systems has been presented to improve the performance of a single classifier. Thus, three decision combination algorithms have been implemented to produce a multiple neural network classifier system. Here the applicability of the system is assessed using patient records in two medical domains. The first task is the prognosis of patients admitted to coronary care units; whereas the second is the prediction of survival in trauma patients. The results are compared with those from logistic regression models, and implications of the system as a useful clinical diagnostic tool are discussed.

7.5. Modular Neural Network

Huai Li et al. [52] developed a method, based on the enhanced segmentation of suspicious mass areas, further development of computer-assisted mass

detection may be decomposed into three distinctive machine learning tasks: 1) construction of the featured knowledge database; 2) mapping of the classified and/or unclassified data points in the database; and 3) development of an intelligent user interface. Decision support system may then be constructed as a complementary machine observer that should enhance the radiologist's performance in mass detection. A mathematical feature extraction procedure is used to construct the featured knowledge database from all the suspicious mass sites localized by the enhanced segmentation. The optimal mapping of the data points is then obtained by learning the generalized normal mixtures and decision boundaries, and developed to carry out both soft and hard clustering. A visual explanation of the decision making is further invented as a decision support, based on an interactive visualization hierarchy through the probabilistic principal component projections of the knowledge database and the localized optimal displays of the retrieved raw data. A prototype system is developed and pilot tested to demonstrate the applicability of this framework to mammographic mass detection.

7.6. Neuro-Fuzzy

Grohman and Dhawan [137] reported that there are many different criteria for the comparative analysis of pattern classifiers. They include generalization ability, computational complexity and understanding of the feature space. A novel convex-set-based neuro-fuzzy algorithm for classification of difficult-to-diagnose instances of breast cancer is described. With its structural approach to feature, space the new method offers rational advantages over the backpropagation algorithm. The classification performance, computational and structural efficiencies are analyzed and compared with that of the BP network. The training procedure is completely automated—function parameters are automatically computed from statistical distributions of the data. Two different approaches to construction of fuzzy membership functions were tested: sigmoidal decision surfaces - (backpropagation-like approach) and bell-shaped functions - cluster-specific approach.

The main idea behind the described method comes from the basic properties of feed forward artificial neural networks. Any layer of a feed forward network performs partitioning of its d -dimensional input feature space into a specific number of subspaces that are always convex and which number can be estimated. This is regardless of the training algorithm or the neural function f used. The only requirement is that the connection weights w_i is linear, i.e., that the relationship between the layer's inputs x_i and the post-synaptic signal processed by the neural function is of a form

$$\varphi = \sum_{i=1}^d x_i w_i + w_0$$

Most popular feed forward networks, including radial basis function and backpropagation, satisfy this

requirement. For $\varphi = 0$ (or any other constant), the above synaptic equation represents a $(d-1)$ -dimensional hyperplane H in the d -dimensional input space separating two regions defined by the connection weights w_i

$$(H: \varphi = 0 \Rightarrow (H: \sum_{i=1}^d x_i w_i + w_0 = 0))$$

Each network layer comprises many such hyper planes, which by intersecting with one another create a finite number of the aforementioned convex subspaces. Therefore, there is a direct relationship between the connection weight values and the obtained d -dimensional convex subspaces. The process of network training could be seen as the attempt at finding an optimal dichotomy of the input space into these convex regions. Moreover, the relationship goes both ways, i.e. proceeding in the reverse order; one might say that finding the optimal dichotomy of the input space into convex subspaces is equivalent to network training.

7.7. Support Vector Machines (SVM)

Yilmaz et al. [142] investigated an approach based on Support Vector Machines (SVMs) for detection of microcalcification (MC) clusters in digital mammograms, and a successive enhancement-learning scheme for improved performance. SVM is a machine-learning method, based on the principle of structural risk minimization, which performs well when applied to data outside the training set. Then formulate microcalcification detection as a supervised-learning problem and apply SVM to develop the detection algorithm. SVM is used to detect at each location in the image whether a microcalcification is present or not. The ability of SVM to outperform several well-known methods developed for the widely studied problem of microcalcification detection suggests that SVM is a promising technique for object detection in a medical imaging application.

7.8. Fuzzy-Nearest Neighbor Classifier

Sekar et al. [53] investigated the fuzzy –nearest neighbor (F-NN) classifier as a fuzzy logic method. That provides a certainty degree for prognostic decision and assessment of the markers, and to compare it with: 1) logistic regression as a statistical method and 2) multiplayer feed forward backpropagation neural networks an artificial neural-network tool, the latter two techniques having been widely used for oncological prognosis. In order to achieve this aim, breast and prostate cancer data sets are considered as benchmarks for this analysis. The overall results indicated that the FK-NN-based method yields the highest predictive accuracy, and that it has produced a more reliable prognostic marker model than the statistical and artificial neural-network-based methods. This is further compared to the LR and MLFFBPNN methods, which have been widely used for predictive analysis in oncology. The results presented show that the FK-NN technique yields the highest predictive accuracy. In

addition, it has also produced a more reliable model as far as marker stratification is concerned. This method not only predicts a class of prognosis, as does MLFFBPNN, but also assigns a confidence degree for each predicted class.

7.9. Fuzzy K-nearest Neighbor (FK-NN) Classifier

The FK-NN is defined as a function of the number of neighborhoods K , class membership degrees, and distances between a pattern to be classified and patterns. A class membership degree between 0 and 1 is computed using the first K minimum distances and the known class membership degrees of the patterns.

The FK-NN algorithm has the similar computation procedure as in a classical k -nearest neighbor algorithm. They enable distances between an unlabeled pattern (i.e., a patient's record), (x) , whose class has to be determined, and patterns (x_k) whose classes (u_{ck}) are previously known ordered in an ascending fashion. In FK-NN the membership degree $(\mu_c(x))$ of an unlabeled pattern for class c is computed using the first k distances as:

$$\mu_c(x) = \left[\frac{\sum_{k=1}^K u_{ck} (1 / (\|x - x_k\|)^{2/(m-1)})}{\sum_{k=1}^K (1 / (\|x - x_k\|)^{2/(m-1)})} \right]$$

where K is the number of neighborhoods selected, and m determines a level of fuzziness. The FK-NN not only gives a class to which the pattern is assigned, but also the class membership degree that provides information about the certainty of the classification decision. One of the main issues related to the FK-NN algorithm is the choice of the number of neighborhoods. This number must be much smaller than the minimum of the number of samples in a class; otherwise, the neighborhood no longer becomes the local neighborhood of a pattern. Since it is difficult to select a value for k , a priori, it is generally determined by a user according to experimental results, and is generally selected as the one that yields the highest predictive accuracy.

7.10. Convolution Neural Network (CNN)

Shainer et al. [114] investigated the classification of regions of interest (ROI's) on mammograms as either mass or normal tissue using a convolution neural network (CNN). A CNN is a backpropagation neural network with two-dimensional (2-D) weight kernels that operate on images. A generalized, fast and stable implementation of the CNN was developed. The input images to the CNN were obtained from the ROI's using two techniques. The first technique employed averaging and sub sampling. The second technique employed texture feature extraction methods applied to small sub regions inside the ROI. Features computed over different sub regions were arranged as texture images, which were subsequently used and CNN inputs. The effects of CNN architecture and texture feature parameters on classification accuracy were studied. ROC methodology was used to

evaluate the classification accuracy. Although classification performance needs to be further improved in order for the classifier to be useful in a clinical setting, it indicates that a CNN can be trained to effectively classify masses and normal breast tissue on mammograms.

Gurcan et al. [88] developed a computer program to detect microcalcification clusters automatically on digitized mammograms. They found that a properly selected and trained convolution neural network (CNN) could reduce false-positive (FP) findings and therefore improve the accuracy of microcalcification detection. In the current study, they evaluated the effectiveness of the CNN optimized with an automated optimization technique in improving the accuracy of the microcalcification detection program, comparing it with the manually selected CNN. The results indicated that the choice of CNN input images is more important than the choice of CNN architecture. Although classification performance needs to be further improved in order for the classifier to be useful in a clinical setting, this study indicates that a CNN can be trained to effectively classify masses and normal breast tissue on mammograms. We are currently investigating the effectiveness of the CNN classifier for differentiation of masses and normal ROI's obtained with an automatic extraction algorithm as a step toward a fully automated computer-aided diagnosis scheme.

7.11. Radial-Basis-Function Neural Network (RBF NN)

Gurcan et al. [88] In order to improve the costs benefits ratio of breast cancer (BC) screenings, evaluated the performance of a back-propagation Artificial Neural Network (ANN) to predict an outcome (cancer: not cancer) to be used as classifier. Networks were trained on data from familial history of cancer, and sociodemographic, gynecobstetric and dietary variables.

Christoyani et al. [54] presented a complete method for fast detection of circumscribed mass in mammograms employing an RBFNN. In this method, each neuron output is a nonlinear transformation of a distance measure of the neuron weights and its input vector. The non-linear operator of the RBFNN hidden layer is implemented using a Cauchy-like probability density function. Successful RBFNN implementation can be achieved using efficient supervised or unsupervised learning algorithms for an accurate estimation of the hidden layer weights. In this implementation, the K-means unsupervised algorithm was used to estimate the hidden-layer weights from a set of training data containing statistical features from both circumscribed lesions and normal tissue. After the initial training and the estimation of the hidden-layer weights, the weights in the output layer are computed using Wincer-filter theory, or equivalently, by minimizing the

mean square error (MSE) between the actual and the desired filter output.

7.12. ANN Pruning

Rudy Setiono et al. [111] developed a new algorithm for neural network pruning. Using this algorithm, networks with small number of connections and high accuracy rates for breast cancer diagnosis are obtained. Then describe how rules can be extracted from a pruned network by considering only a finite number of hidden unit activation values. The accuracy of the extracted rules is as high as the accuracy of the pruned network. For the breast cancer diagnosis problem, the concise rules extracted from the network achieve an accuracy rate of more than 95% on the training data set and on the test data set. This algorithm allows us to consider only a small number of different hidden unit activation values and still maintain the accuracy of the original network.

7.13. Self-Organizing Map (SOM)

Markey et al. [90] identified and characterized clusters in a heterogeneous breast cancer computer-aided diagnosis database. Identification of subgroups within the database could help elucidate clinical trends and facilitate future model building. A self-organizing map (SOM) was used to identify clusters in a large (2258 cases), heterogeneous computer-aided diagnosis database based on mammographic findings (BI-RADSTM) and patient age.

A self-organizing map relates similar cases (input vectors) to the same region of a map of Neurons. The SOM was computed using the SOM toolbox in MATLAB (The MathWorks Inc., Natick, MA). The basic SOM consisted of 16 neurons arranged in a single layer in a 2-D square grid of 4×4 neurons, but different configurations were considered. For each case, the Euclidean distance between the case and each neuron was calculated based on the seven input features (the biopsy outcome was not provided to the SOM). For input to the SOM, each feature was scaled by subtracting the mean and dividing by the standard deviation, resulting in each scaled feature having mean zero and standard deviation of one. After the most similar neuron was determined, the neurons in its neighborhood were identified. The neighborhood of a neuron was defined as all the neurons within a given link distance of the matched neuron. All the neurons in the neighborhood were adjusted to have feature values closer to the current case. The amount that the neuron weights were adjusted was controlled by the learning rate. The learning rates and distance threshold values used were the default values for the SOM toolbox.

7.14. Constraint Satisfaction Neural Network (CSNN)

After the clusters were identified, a CSNN was used to determine the profiles of the clusters. The Lyapunov energy function was used as a measure of the

network stability. It was found that 1000 iterations were sufficient to achieve stability. The weights were predetermined using auto associative backpropagation neural networks (auto-BP). The auto-BP networks were trained with a learning rate of 1.0 for 100 iterations and the root mean squared training error was approximately 0.1 (network outputs between 0 and 1). For each cluster, a CSNN was used to generate a profile. Each category of the categorical BI-RADS features corresponded to a binary variable and associated neuron. For example, the mass margin with its five non-zero categories was represented by five separate neurons. Patient age was translated into a discrete variable with five levels (<40 years, $40 \leq x < 50$, $50 \leq x < 60$, $60 \leq x < 70$, ≥ 70 years). An additional neuron was used to signify cluster membership. The activation level of the neuron indicating cluster membership was set to the maximal value and the other neurons were allowed to evolve until the network reached a stable state. The feature neurons that were activated defined the profile of the cluster. A profile is a list of feature values that succinctly summarizes the cluster and defines a "typical" case (e.g. mass margin is well circumscribed, mass shape is round, and patient age is between 50 and 60 years). All cases in the cluster do not exactly match the profile; there is still a distribution of feature values. Notice that unlike common summary statistics, such as the cluster centroid, the CSNN profile implicitly includes feature selection; only features deemed relevant to the network for describing a cluster are included.

7.15. Back-Propagation Artificial Neural Network (BP-ANN)

A feed-forward back-propagation artificial neural network (BP-ANN) was used to predict the biopsy outcome from the mammographic findings and patient age [2]. The BPANN was trained to minimize the sum-of-squares error using the back-propagation algorithm. The network had a single hidden layer of 14 neurons and each neuron in the network used a logistic activation function. The network inputs (7) were the BI-RADS features and patient age. Network inputs were rescaled from 0 to 1 (by subtracting the minimum value and dividing by the maximum minus the minimum). The biopsy outcomes were the network targets; there was one output node indicating malignancy. The 2258 cases were presented to the network in a round-robin manner (leave-one out, k-fold cross-validation with $k = N$) and training ended before the average testing error on the left-out cases began to increase.

7.16. Mixed Feature Based Neural Network (MFNN)

Zheng et al. [152] presented a computationally efficient mixed feature based neural network (MFNN) for the detection of Microcalcification Clusters (MCC's) in digitized mammograms. The MFNN employs features computed in both the spatial and spectral

domain and uses spectral entropy as a decision parameter. Backpropagation with Kalman Filtering (KF) is employed to allow more efficient network training as required for evaluation of different features, input images, and related error analysis. A wavelet-based image-enhancement method is also employed to enhance microcalcification clusters for improved detection. The relative performance of the MFNN for both the raw and enhanced images is evaluated using a common image database of 30 digitized mammograms, with 20 images containing 21 biopsy proven MCC's and 10 normal cases.

The computed sensitivity (true positive (TP) detection rate) was 90.1% with an average low false positive (FP) detection of 0.71 MCCs/image for the enhanced images using a modified k-fold validation error estimation technique. The corresponding computed sensitivity for the raw images was reduced to 81.4% and with 0.59 FP's MCCs/image. A relative comparison to an earlier neural network (NN) design, using only spatially related features, suggest the importance of the addition of spectral domain features when the raw image data is analyzed. Two sets of features are computed, one set in the spatial domain and the other set in the spectral domain. The intent is to compute these features from both the raw and wavelet based enhanced images. The features, in turn, are computed within images block that contain either microcalcifications or normal tissues. Then these features are applied to MFNN.

7.17. Enhanced Rough Set Approach

Aboul Ella Hassanien and J.M. Ali [1] presented an enhanced rough set approach for attribute reduction and generating classification rules from digital mammogram. The classifier model was built and quadratic distances similarly; function is used for matching process. To evaluate the validity of the rules based on the approximation quality of the attributes, a statistical test is made to evaluate the significance of the rules. The experimental results show that the classification algorithm performs well, reaching over 93% in accuracy with less number of rules compared with a well-known decision trees and neural network classifier models.

8. Result Analysis

Result analysis is based on ROC and FROC

8.1 ROC and FROC curve analysis

Another measure of performance is the Receiver Operating Characteristic (ROC) curve. ROC curves measure predictive utility by showing the tradeoff between the true-positive rate and the false-positive rate inherent in selecting specific thresholds on which predictions might be based. The area under this curve represents the probability that, given a positive case and

a negative one, the classifier rule output will be higher for the positive case and it is not dependent on the choice of decision threshold.

Table 5. Overview of Classifiers

References	Methods	Remarks
[139]	Binary decision tree	Area under ROC curve 0.9, 24 images, source N/A
[139]	Quadratic Classifier	Area under ROC curve 0.918 on 24 images, source N/A
[12]	Linear classifier	Maximum area 0.70 under ROC, 70 images, source N/A
[30,31]		TPF: 100% and FP: 5c/f, 50 images, source N/A
[102]		TPF: 85% and FP: 1.5c/f, 78 images, source N/A
[139]		Area under ROC curve 0.936, 24 images, source N/A
[101]		TPF: 85% and FP: 2.5c/f, 78 images, source N/A
[99,100]		TPF: 85%, FP: 2c/f, 78 images, source N/A
[114]	Convolution neural network	T.P. 90% from 168 Mammograms
[111]	Neural network pruning	T.P. 95%
[68]	Adaptive resonance theory, linear discriminant classifier	78 X-ray mammograms
[10]	Fuzzy decision tree	Specificity: 73% and sensitivity: 60%, 118 images, source N/A
[28]	Artificial neural networks	216 images (111 malignant, 105 benign)
[1]	Back-propagation artificial neural network	T.P. 94.04%
[84,85]	Quadratic classifier	Incorrect: 7.05%, Correct: 40%, Undecided: 52.86%, close to the mean performance of three expert radiologists 146 images, source N/A
[54]	RBFNN	TP: 72.72%
[25]	Multiple expert system	The area under the ROC curve is 0.786, 40 images for USF
[77]	Fractal analysis, DWT	97.3% of sensitivity, FP: 3.92, for 322 images from MIAS.
[52]	Modular NN	Sensitivity: 181/186
[142]	Support vector machines	TP: 67%
[106]	Rule-based and a neural network sub-system	Specificity is 1.80, FP: 1.15 for the Nijmegen and MIAS
[88]	Convolution neural network, averaging, subsampling, SGLD	T.P.: 93.3%. F.P. 0.7
[53]	Fuzzy -nearest neighbor (FK-NN) classifier	
[90]	Self-organizing map, constraint satisfaction neural network	T.P. 79%
[2]	FEM with ANN	TP: 87%, TN: 83%, CC: 93%
[83,84]	Neural Networks	Maximum area 0.86 under ROC, source N/A
[41]		TP: 90.6% on 128 ROIs, source N/A
[138]		90% TP, and less than half of the test images showing false images. 9 images: 288 samples with 144 for each class, source N/A
[139]		Area under ROC curve 0.935, 24 images, source N/A
[5]		TP 93% and FP: 1.5 c/f 27 images, source N/A
[37]		Maximum area 0.76 under ROC, 191 images, source N/A
[152]		TPF: 90% and FP: 0.77% on 30 images, source N/A
[87]		TPF: 100% on MCC on 24/MCC, source N/A
[18]		TPF: 90% and FP: 1% 40 images in Nijmegen database
[115]		Detection Rate: 88.89%. 5 images, source N/A
[87]		TP: 90% and FP: 1.2c/f, 40 images in Nijmegen database
[43]		88% correct rate in the test case of 200 images in USF database
[67]		The area under ROC curve is 0.88, 120 images, source N/A
[146]		93% mean TPF and FP 1c/f, 40 images in Nijmegen database
[110]		100% sensitivity and 41.6% specificity the corresponding radiologists is 89% and 58.3% in 40 images in LLNLUCSF
[145]		90% mean TPF and FP 0.5c/f on 40 images in Nijmegen database
[149]		TPF: 97.6% and FPF: 3.15c/f on 63 images in USUHS database
[11]		TP: 88.9%; 40 images in Nijmegen database
[14]	K-Nearest Neighbor Classifier	TP: 80% and FP: 1 c/f, test image is generated by computer simulation
[139]		Area under ROC curve 0.929, 24 images, source N/A
[50]		TPF: 100% and FP: 0.23 c/f, 80% correct rate and 0.25 c/f FP, 150 images from MIAS database
[65]		Discussion is given on different parameter set, 245 images, source N/A
[108]		TP: 85% and 0.1 FP, 40 images in Nijmegen database
[71]		More than 80% classification accuracy on 180 images in Nijmegen LLNLUCSF database
[7]		TP: 93.48 and FP: 1.09% on 32 images in Nijmegen database
[12]	Bayesian classifier	The agreement between this classifier and the radiologists is 84% on 70 images, source N/A
[62]		TP: 92% with FP: 1c/f, 65 images, source N/A

ROC analysis is based on statistical decision theory, developed in the context of electronic signal detection, and has been applied extensively to diagnostic systems in clinical medicine. The ROC curve is a plot of the classifier's true positive detection rate versus its false positive rate. The false positive (FP) rate is the probability of incorrectly classifying a non-target object (e.g. normal tissue region) as a target object (e.g. tumor region). Similarly, the true positive (TP) detection rate is the probability of correctly classifying a target object as being a target object. The TP and FP rates both are specified in the interval from 0.0 to 1.0, inclusive, in medical imaging, the TP rate is referred to as sensitivity, and $(1.0 - \text{FP rate})$ is called specificity. Statistical classifiers have parameters that can be varied to alter the TP and FP rates. Using these parameters, an ROC curve can be generated which shows the TP/FP trade-off associated with the different values that the parameter(s) may assume. It would be possible to trade a lower (higher) FP rate for a higher (lower) TP detection rate by choosing appropriate value(s) for the parameter(s) in question.

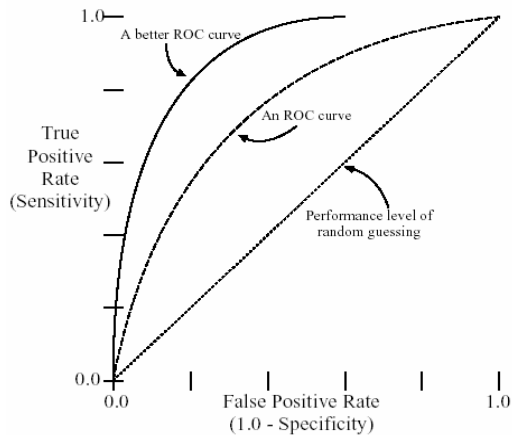


Figure 8.1. An Example of Two typical ROC Curves

A typical ROC curve is shown in Figure 8.1. The Area under the ROC curve (AUC) is an accepted way of comparing classifier performance [127,89]. A perfect classifier would have a TP rate of 1.0 (or 100%) and a FP rate of 0.0 and therefore would have an AUC of 1.0. Random guessing would result in an AUC of 0.5. When the different possible errors that can be made by the classifier have different “costs” then “profits” can be maximized by selecting the appropriate operating point on the ROC curve. In practical application, this requires that the underlying parameters of the classifier be easily manipulated to facilitate selection of the ROC operating point [47].

The AUCs are estimated by using the trapezoid rule for the discrete operating points. The AUC can also be computed by fitting a continuous

binormal curve to the operating points, requiring an assumption to be made about the functional form of the ROC curve [89]. This type of curve fitting is generally done for medical imaging studies when operating points are obtained by presenting a reader with normal and abnormal images in random order, and the reader is asked to rank each image on a discrete ordinal scale of 5 or 6 categories ranging from definitely normal to definitely abnormal [45,46,89,127]. This is known as a confidence rating. The ROC points are obtained by successively considering broader and broader categories of abnormal. In other words, thresholds are labeled abnormal. While any images rated below the threshold are labeled normal.

For evaluating true-positive detection, sometimes it is required not only the existence but also the localization of the tumor. A better method for this case is FROC analysis that is a plot of operating points showing the tradeoff between the TP rates versus the average number of false positives per image. However, both FROC and ROC analysis suffer from their limitations. For instance, they do not address the complexity of images and are difficult to transform the subjective measurements (radiologist's observations) to the objective FROC curve.

Zwiggelaar et al. [109] described methods for detecting linear structures in mammograms, and for classifying them into anatomical types (vessels, spicules, ducts, etc). Several different detection methods are compared, using realistic synthetic images and ROC analysis.

8.2 Sensitivity versus Specificity:

The use of the overall classification accuracy as an evaluation metric is adequate provided the class distribution among examples is constant and relatively balanced. Furthermore, this evaluation approach also assumes equal error costs, *i.e.* that a false positive error is equally significant as a false negative error. Unfortunately, in real-life problems, these assumptions are not always true. Consequently, the performance of such systems is best described in terms of their *sensitivity* and *specificity* quantifying their performance related to false positive and false negative instances. These metrics are based on the consideration that a test point always falls into one of the following four categories:

- False Positive (FP) if the system labels a negative point as positive;
- False Negative (FN) if the system labels a positive point as negative;
- True Positive (TP) and
- True Negative (TN) if the system correctly predicts the label.

The sensitivity or true positive rate of a learning machine is defined as the ratio between the number of true positive predictions TP and the number of positive instances in the test set. It is defined as follows:

$$\text{Sensitivity} = T_P / (T_P + F_N)$$

While, the specificity or true negative rate is defined as the ratio between the number of true negative predictions TN and the number of negative instances in the test set. It is defined as follows:

$$\text{Specificity} = T_N / (T_N + F_P)$$

The overall accuracy is the ratio between the total number of correctly classified instances and the test set size. It is defined as follows:

$$\text{Overall Accuracy} = (N_r / N) * 100 \%$$

Where, N_r is the number of correctly classified samples during the test run and N is the complete number of test samples.

8.3 Metrics

Recent prospective studies have suggested that user's confidence in computer-aided detection (CAD) marks and their tolerance of false positive (FP0) marks play a role in the benefit gained from a CAD device [141]. To introduce new metrics to improve the characterization of the latest generation of CAD algorithms and to describe the algorithm performance tradeoffs with user adjustable operating points. As CAD algorithms continue to improve, the new measurements presented. Provide the user with more information and a more accurate assessment of CAD system performance, while user determined operating points allow for tailored/individualized incorporation of CAD into the reading environment.

9. Conclusions

Automated breast cancer detection has been studied for more than two decades. This survey was conducted in order to establish a roadmap that is able to forecast the future developments of image processing technology in medicine and healthcare. In this paper, we have examined various steps in detection of microcalcifications (1) the pre processing and enhancement, (2) bilateral subtraction techniques, (3) segmentation algorithms, (4) features extraction, selection and classification, (5) classifiers, (6) Receiver Operating Characteristic (ROC); Free-response Receiver Operating Characteristic (FROC) analysis and their performances were studied and compared.

We have described a comprehensive of methods in a uniform terminology, to define general properties and requirements of local techniques, to enable the readers to select the efficient method that is optimal for the specific application in detection of microcalcifications in mammogram images. Although

by now some progress has been achieved, there are still remaining challenges and directions for future research, such as, developing better preprocessing, enhancement and segmentation techniques; designing better feature extraction, selection and classification algorithms; integration of classifiers to reduce both false positives and false negatives; employing high resolution mammograms and investigating 3D mammograms. The CAD mammography systems for microcalcifications detection have gone from crude tools in the research laboratory to commercial systems.

Several commercial companies such as R2 Technology Inc., Hewlett Packard Co., Sterling Diagnostic Imaging, Siemens, General Electric, Med Detect/Lockheed Martin, were developing or designing mammography systems for clinical applications. R2 Technology Inc. has produced a system Image Checker for microcalcifications and mass detection. In order to reduce false positive, several different types of features, sometimes, with clinical information should be used. As the complexity of algorithm increases, the time complexity of the CAD will also increase.

Mammogram image analysis society database is standard test set but defining different standard test set (database) and better evaluation criteria are still very important. With some rigorous evaluations, and objective and fair comparison could determine the relative merit of competing algorithms and facilitate the development of better and robust systems.

ACKNOWLEDGEMENT

The first author sincerely acknowledges the University of Grant Commission (UGC) for extending the financial support under UGC special assistance programme, New Delhi, India

REFERENCES

- [1] Aboul Ella Hassanien and J.M. Ali, "Enhanced Rough Sets Rule Reduction Algorithm for Classification Digital Mammography", *Intelligent System journal*, UK, Freund & Pettman, pp: 151-171, v. 13, n. 2, 2004.
- [2] Alvaro L. Ronco, "Use of Artificial Neural Networks in Modeling Associations of Discriminant Factors: Towards an Intelligent Selective Breast Cancer Screening", *Artificial Intelligence in Medicine*, pp: 299-309, v.16 1999.
- [3] M.A. Anastasio, H. Yoshida, R. Nagel, R.M. Nishikawa, K. Doi, "A genetic algorithm-based method for optimizing the performance of a computer-aided diagnosis scheme for detection of clustered microcalcifications in mammograms", *Med. Phys.* pp: 1613-1620, v.25, n.9, 1998.

- [4] Antony Jalink, James McAdoo, Gary Halama, and Hong Liu, "CCD Mosaic Technique for Large-Field Digital Mammography", *IEEE Transactions on Medical Imaging*, pp: 260–267, v.15, n.3, 1996.
- [5] Bankman, J. Tsai, D. Kim, O. Gatewood, W. Brody, "Detection of microcalcification clusters using neural networks", *Annual International Conference of the IEEE Engineering in Medicine and Biology Society—Proceedings*, pp: 590–591, v.16, 1994.
- [6] Berkman Shainer, Member, IEEE, Heang-Ping Chan, Nicholas Petrick, Datong Wei, Mark A. Helvie, Dorit D. Adler, and Mitchell M. Goodsitt, "Classification of Mass and Breast Tissue: A Convolution Neural Network Classifier with Spatial Domain and Texture Images", *IEEE Transactions on Medical Imaging*, pp: 598–610, v.15, n.5, 1996.
- [7] T. Bhangale, U.B. Desai, U. Sharma, "An unsupervised scheme for detection of microcalcifications on mammograms", *IEEE International Conference on Image Processing*, pp: 184–187, 2000.
- [8] L. Bocchi, G. Coppini, J. Nori, G. Valli, "Detection of Single and Clustered Microcalcifications in Mammograms Using Fractals Models and Neural Networks", *Medical Engineering & Physics*, pp: 303 – 312, v. 26, 2004.
- [9] Boris Kovalerchuk, Evangelos Traintaphyllou, James F. Ruiz, Jane Clayton, "Fuzzy Logic in Computer-Aided Breast Cancer Diagnosis: Analysis of Lobulation", *Artificial Intelligence in Medicine*, pp: 75–85, v.11, 1997.
- [10] S. Bothorel, B.B. Meunier, S.Muller, "A fuzzy logic based approach for semiological analysis of microcalcifications in mammographic images", *Int. J. Intelligent Systems*, pp: 819–848, v.12, 1997.
- [11] Brijesh Verma and John Zakos, "A Computer-Aided Diagnosis System for Digital Mammograms Based on Fuzzy-Neural and Feature Extraction Techniques", *IEEE Transactions on Information Technology in Biomedicine*, pp: 46–54, v.5, n.1, 2001.
- [12] C.B. Caldwell, S.J. Stapleton, D.W. Holsworth, R.A. Jong, "Characterization of mammographic parenchymal pattern by fractal dimension", *Phys. Med. Biol.*, pp: 235–247, v. 35, n.2, 1990.
- [13] Carlos Andres Pena-Reyes, Moshe Sipper, "A Fuzzy-Genetic Approach to Breast Cancer Diagnosis", *Artificial Intelligence in Medicine*, pp: 131– 55, v.17, 1999.
- [14] H.P. Chan, K. Doi, S. Galhotra, C.J. Vyborny, H. MacMahon, P.M. Jokich, "Image feature analysis and computer-aided diagnosis in digital radiography I. Automated detection of microcalcifications in mammography", *Med. Phys.*, pp: 538–548, v.14, n.4, 1987.
- [15] H.P. Chan, B. Sahiner, K.L. Lam, "Computerized analysis of mammographic microcalcifications in morphological and texture features space", *Med. Phys.*, pp: 2007–2019, v.25, 1998.
- [16] H.P. Chan, Vyborny C.J., McaMahon H., C.E. Metz, K. Doi, E.A. Sickles, "Digital mammography: ROC studies of the effects of pixel size and unship-mask filtering on the detection of subtle microcalcifications", *Invest. Radiol.*, pp: 581–589, v.22, n.7, 1987.
- [17] Chee Peng Lim, Robert F. Harrison, R. Lee Kennedy, "Application of autonomous neural network systems to medical pattern classification tasks", *Artificial Intelligence in Medicine*, pp: 215-239, v.11, 1997.
- [18] C.H. Chen, G.G. Lee, "Image segmentation using multiresolution wavelet analysis and expectation-maximization (EM) algorithm for digital mammography", *J. Digital Imag.*, pp: 491–504, v.8, 1997.
- [19] H. D. Cheng, Jingli Wang, Xiangjun Shi, "Microcalcification Detection Using Fuzzy Logic and Scale Space Approaches", *Pattern Recognition*, pp: 363–375, v.37, 2004.
- [20] H.D. Cheng, Xiaopeng Cai, Xiao Wei Chen, Liming Hu, Xueling Lou, "Computer-Aided Detection and Classification of Microcalcifications in Mammograms: A Survey", *Pattern Recognition*, pp: 2967–2991, v.36, 2003.
- [21] H.D. Cheng, J.R. Chen, R.I. Freimanis, X.H. Jiang, "A novel fuzzy logic approach to microcalcification detection", *J. Inform. Sci.*, pp: 1-14, 1998.
- [22] H.D. Cheng, Y.M. Lui, R.I. Freimanis, "A novel approach to microcalcification detection using fuzzy logic technique", *IEEE Trans. Med. Imag.*, pp: 442–450, v.17, n.3, 1998.
- [23] T.W. Cheng, D.B. Goldgof, L. Hall, "Fast fuzzy clustering", *Fuzzy Sets and Systems*, pp: 49–56, v.93, 1998.
- [24] Chun-Ming Chang and Andrew Laine, "Coherence of Multiscale Features for Enhancement of Digital Mammograms", *IEEE Transactions on Information Technology in Biomedicine*, pp: 32 – 46, v.3, n.1, 1999.
- [25] L.P. Cordella, F. Tortorella, M. Vento, "Combing experts with different features for classifying clustered microcalcifications in mammograms", *Proceedings of 15th International Conference on Patten Recognition*, pp: 324–327, 2000.
- [26] Dani Kramer, Farzin Aghdasi, "Texture analysis techniques for the classification of microcalcifications in digitized mammograms", *Proceedings of the 1999 Fifth IEEE AFRICON Conference Electro technical Service for Africa*, pp: 395–400, 1999.

- [27] J.S. DaPonte, P. Sherman, "Classification of ultrasonic image texture by statistical discriminant analysis and neural networks", *Comput. Med. Imag. Graphics*, pp: 3–9, v. 15, n.1, 1991.
- [28] David B. Fogel, Eugene C. Wasson III, Edward M. Boughton, Vincent W. Porto, "Evolving Artificial Neural Networks for Screening Features from Mammograms", *Artificial Intelligence in Medicine*, pp: 317 – 326, v. 14, 1998.
- [29] David B. Fogel, Eugene C. Waston, Edward M. Boughton, Vincent W. Porto, and Peter J. Angeline, "Linear and Neural Models for Classifying Breast Masses", *IEEE Transactions on Medical Imaging* 17(3) (1998b) 485 – 488.
- [30] D.H. Davies, D.R. Dance, "Automatic computer detection of clustered calcifications in digital mammograms", *Phys. Med. Biol.* 35 (1990a) 1111–1118.
- [31] D.H. Davies, D.R. Dance, C.H. Jones, "Automatic detection of clusters of calcifications in digital mammograms", *SPIE Med. Imag. IV: Image Process*, pp: 185–191, v. 1233, 1990.
- [32] D.H. Davies, D.R. Dance, "The automatic computer detection of subtle calcifications in radiographically dense breasts", *Phys. Med. Biol.*, pp: 1385–1390, v.37, 1992.
- [33] J. Dengler, S. Behrens, J.F. Desaga, "Segmentation of microcalcifications in mammograms", *IEEE Trans. Med. Imag.*, pp: 634–642, v.12, n.4, 1993.
- [34] S.B. Desai, M.T. Moonim, Amarinder K. Gill, Rahpal Singh Punia, K.N. Naresh and R.F. Chinoy, "Hormone Receptor Status of Breast Cancer in India: A Study of 798 Tumors", *Department of Pathology, Tata Memorial Hospital, Mumbai – 400 012, India. The Breast*, pp: 267 – 270, v.9, 2000.
- [35] A.P. Dhawan, G. Buellton, R. Gordon, "Enhancement of mammographic features by optimal adaptive neighborhood image processing", *IEEE Trans. Med. Imag.*, pp: 8–15, v.MI-5, n.1, 1986.
- [36] A.P. Dhawan, Y. Chitre, C. Bonasso, K. Wheeler, "Radial-basis-function based classification of mammographic microcalcifications using texture features", *IEEE Proceedings of the 1995 IEEE Engineering in Medicine and Biology 17th Annual Conference and 21st Canadian Medical and Biological Engineering Conference*, pp: 535–536, 1995.
- [37] A.P. Dhawan, Y. Chitre, C. Kaiser-Bonasso, M. Moskowita, "Analysis of mammographic microcalcifications using grey-level image structure features", *IEEE Trans. Med. Imag.*, pp: 246–259, v.15, n.3, 1996.
- [38] S. Dippel, M. Stahl, R. Wiemker, T. Blaffert, "Multiscale contrast enhancement for radiographies: Laplacian pyramid versus fast wavelet transform", *IEEE Trans. Med. Imag.*, pp: 343–353, v.21, n.4, 2002.
- [39] C.Y. Enderwich, E.M. Tzanakou, "Classification of mammographic tissue using shape and texture features", *Proceedings of the 19th International Conference-IEEE/EMBS*, pp: 810–813, 1997.
- [40] B.W. Fam, S.L. Olson, P.F. Winter, F.J. Scholz, "Algorithm for the detection of fine clustered calcifications on film mammograms", *Radiology*, pp: 333–337, v.169, n.2, 1988.
- [41] R. J. Ferrari, Member, IEEE, R.M. Rangayyan, Fellow, IEEE, J.E.L. Desautels, R.A. Borges, and A.F. Frere, "Automatic Identification of the Pectoral Muscle in Mammograms", *IEEE Transaction on Medical Imaging*, pp: 232 – 245, v.23, n.2, 2004.
- [42] R. J. Ferrari, R.M. Rangayyan, J.E.L. Desautels, and A.F. Frere, "Analysis of Asymmetry in Mammograms via Directional Filtering With Gabor Wavelets", *IEEE Transactions on Medical Imaging*, pp: 953–964, v.20, n.9, 2001.
- [43] R.J. Ferrari, A.C.P.L.F. de Carvalho, P.M.A. Marques, A.F. Frere, "Computerized classification of breast lesions: shape and texture analysis using an artificial neural network", *Image Process. Appl.*, pp: 517–521, 1999.
- [44] Francisco L. Valverde, Nicolas Guil, Jose Munoz, "Segmentation of Vessels from Mammograms Using A Deformable Model", *Computer Methods and Programs in Biomedicine*, pp: 233 – 247, v.73, 2004.
- [45] J.A. Hanley and B.J. McNeil, "A method of comparing the areas under receiver operating characteristic curves derived from the same cases", *Radiology*, pp: 839–843, v.148, 1983.
- [46] J.A. Hanley and B.J. McNeil, "The Meaning and use of the area under a receiver operating characteristic (ROC) curve", *Radiology*, pp: 29–36, v.143, 1982.
- [47] R.M. Haralick and L.G. Shapiro, "Computer and Robot Vision 1", *Addison Wesley*, 1992.
- [48] Hidefurni Kobatake, Member, IEEE, Masayuki Murakami, Hideya Takeo, and Sigeru Nawano, "Computerized Detection of Malignant Tumors on Digital Mammograms", *IEEE Transactions on Information Technology in Biomedicine*, pp: 369–378, v.18, n.5, 1999.
- [49] R.P. Highnam, J.M. Brady, and B.J. Shepstone, "Computing the Scatter Component of Mammographic Images", *IEEE Transactions on Medical Imaging*, pp: 301–313, v.13, n.2, 1994.
- [50] S.A. Hojjatoleslami, J. Kittler, "Detection of clusters of microcalcification using a K-nearest neighbor classifier", *Proceedings of the 1996 IEE Colloquium on Digital Mammography*, pp: 1–6, 1996.
- [51] Huai Li, Member, IEEE, K. J. Ray Liu, Senior Member, IEEE, and Shih-Chung B. Lo, Member, IEEE, "Fractal Modeling and Segmentation for the Enhancement of Microcalcifications in Digital

- Mammograms”, *IEEE Transactions on Medical Imaging*, pp: 785–798, v.16, n.6, 1997.
- [52] Huai Li, Yue Wang, K.J. Ray Liu, Shih-Chung B. Lo, and Matthew T. Freedman, “Computerized Radiographic Mass Detection – Part II: Decision Support by Feature Database Visualization and Modular Neural Networks”, *IEEE Transactions on Medical Imaging*, pp: 302–313, v.20, n.4, 2001.
- [53] Huseyin Sekar, Student Member, IEEE, Michael O. Odetayo, Dobrila Petrovic, and Raouf N. G. Naguib, Senior Member, IEEE, “A Fuzzy Logic Based Method for Prognostic Decision Making in Breast and Prostate Cancers”, *IEEE Transactions on Information Technology in Biomedicine*, pp: 114 – 122, v.7, n.2, 2003.
- [54] Ioanna Christoyiani, Evalgelos Dermatas, and George Kokkinakis, “Fast Detection of Masses in Computer Aided Mammography”, *IEEE Signal Processing Magazine*, pp: 54–64, 2000.
- [55] Y. Jiang, R.M. Nishikawa, D.E. Wolverton, C.E. Metz, R.A. Schmidt, K. Doi, “Computerized classification of malignant and benign clustered microcalcifications in mammograms”, *Proceedings of 19th International Conference-IEEE/EMBS*, pp: 521–523, 1997.
- [56] H.R. Jin, “Extraction of microcalcifications from mammograms using morphological filter with multiple structuring elements”, *System Comput. Jpn.*, pp: 66–74, v.24, n.11, 1993.
- [57] Joachim Dengler, Sabine Benrens, and Hojann Freidrich Desaga, “Segmentation of Microcalcifications in Mammograms”, *IEEE Transactions on Medical Imaging*, pp: 664–669, v.12, n.4, 1993.
- [58] John J. Heine, Stanely R. Deans, Senior Member, IEEE, D. Kent Cullers, Richard Stauduhar, Member, IEEE, and Laurence P. Clarke, Member, IEEE, “Multiresolution Statistical Analysis of High-Resolution Digital Mammograms”, *IEEE Transactions on Medical Imaging*, pp: 603–515, v.16, n.5, 1997.
- [59] Jong Kook Kim, Jeong Mi Park, Koun Sik Song, and Hyun Wood Park, “Adaptive Mammographic Image Enhancement Using First Derivative and Local Statistics”, *IEEE Transactions on Medical Imaging*, pp: 495–502, v.16, n.5, 1997.
- [60] Jusy Kilday, Francesco Palmieri, and Martin D. Fox, “Classifying Mammographic Lesions Using Computerized Image Analysis”, *IEEE Transactions on Medical Imaging*, pp: 664–669, v.12, n.4, 1993.
- [61] M. Kallergi, K. Woods, L.P. Clarke, W. Qian, R.A. Clark, “Image segmentation in digital mammography: comparison of local thresholding and region growing algorithms”, *Compute. Med. Imag. Graph.*, pp: 323–331, v. 16, 1992.
- [62] N. Karssemeijer, “A stochastic model for automated detection of calcifications in digital mammograms”, *12th International Conference IPMI, Wye, UK*, pp: 227–238, 1992.
- [63] N. Karssemeijer, “Adaptive noise equalization and image analysis in mammography”, *Information Processing in Medical Imaging, 13th International Conference*, pp: 472–486, IPMI ’93, AZ, USA, 1993.
- [64] N. Karssemeijer, “Adaptive noise equalization and recognition of microcalcification clusters in mammograms”, *Int. J. Pattern Recognition Artif. Intell.*, pp: 1357–1376, v.7, n.6, 1993.
- [65] N. Karssemeijer, W.J.H. Veldkamp, “An improved method for detection of microcalcification clusters in digital mammograms”, *The SPIE Conference on Image Processing*, pp: 512–522, v.3661, 1999.
- [66] Kathleen M. Dallesio. “MR Imaging of the Breast”, *Applied Radiology*, pp: 40–41, 2003.
- [67] J.K. Kim, H.W. Park, “Statistical textural features for detection of microcalcifications in digitized mammograms”, *IEEE Trans. Med. Imag.*, pp: 231–238, v.18, n.3, 1999.
- [68] J.K. Kim, J.M. Park, K.S. Song, H.W. Park, “Adaptive mammographic image enhancement using first derivative and local statistics”, *IEEE Trans. Med. Imaging.*, pp: 495–502, v.16, n.5, 1997.
- [69] J.K. Kim, J.M. Park, S.S. Song, H.W. Park, “Detection of clustered microcalcifications on mammograms using surrounding region dependence method and artificial neural network”, *J. VLSI Signal Process.*, pp: 251–262, v.18, 1998.
- [70] C.M. Kocur, S.K. Gogers, L.R. Myers, T. Burns, M. Kabrisky, J.W. Hoffmeister, K.W. Bayer, J.M. Steppe, “Using neural networks to select wavelet features for breast cancer diagnosis”, *IEEE Eng. Med. Biol.*, pp: 95–102, v.15, n.3, 1996.
- [71] D. Kramer, F. Aghdasi, “Classification of microcalcifications in digitized mammograms using multiscale statistical texture analysis”, *Proceedings of the South African Symposium on Communications and Signal Processing*, pp: 121–126, 1998.
- [72] Kristin J. McLoughlin, Philip J. Bones, Senior Member, IEEE, and Nico Karssemeijer, Member, IEEE, “Noise Equalization for Detection of Microcalcification Clusters in Direct Digital Mammogram Images”, *IEEE Transaction on Medical Imaging*, pp: 313–320, v.23, n.3, 2004.
- [73] A.F. Laine, S. Schuler, J. Fan, W. Huda, “Mammographic feature enhancement by multiscale analysis”, *IEEE Trans. Med. Imag.*, pp: 7250–7260, v.13, n.4, 1994.
- [74] A. Lauria, R. Palmierob, G. Forni, M.E. Fantacci, M. Imbriacod, A. Sodanoe, P.L. Indovin, “A Study on Two Different CAD Systems for Mammography as an aid to Radiological Diagnosis in the Search of

- Microcalcification Clusters”, *European Journal of Radiology*, 2004.
- [75] C.S. Lee, J.K. Kim, H.W. Park, “Computer-aided diagnostic system for breast cancer by detecting microcalcification”, *SPIE*, pp: 615–626, v.3335, 1998.
- [76] F. Lefebvre, H. Benali, E. Kahn, R.D. Paola, “A fractal approach to the segmentation of microcalcifications in digital mammograms”, *Med. Phys.*, pp: 381–391, v.22, n.4, 1995.
- [77] Lei Zheng and Andrew K. Chan, Senior Member, IEEE, “An Artificial Intelligent Algorithm for Tumor Detection in Screening Mammogram”, *IEEE Transactions on Medical Imaging*, pp: 559 – 567, v.20, n.7, 2001.
- [78] G. Lemaur, K. Drouiche, and H. DeConinck, “Highly Regular Wavelets for the Detection of Clustered Microcalcifications in Mammograms”, *IEEE Transactions on Medical Imaging*, pp:393–401, v.22, n.3, 2003.
- [79] H.D. Li, M. Kallergi, L.P. Clarke, V.K. Jain, Senior Member, IEEE, and R.A. Clark, “Markov Random Field for Tumor Detection in Digital Mammography”, *IEEE Transactions on Medical Imaging*, pp: 565–576, v.14, n.3, 1995.
- [80] H. Li, K.J.R. Liu, S.C.B. Lo, “Fractal modeling of mammogram and enhancement of microcalcifications”, *IEEE Nuclear Science Symposium & Medical Imaging Conference*, pp: 1850–1854, v.3, 1996.
- [81] Lori Mann Bruce, Member, IEEE, and Reza R. Adhami, Member, IEEE, “Classifying Mammographic Mass Shapes Using the Wavelet Transform Modulus-Maxima Method”, *IEEE Transactions on Medical Imaging*, pp: 1170 –1177, v.18, n.12, 1999.
- [82] A. Malich, T. Boehm, M. Facius, M.G. Fressmeyer, F. Fleck, R. Anderson, W.A. Kaise, “Differentiation of Mammographically Suspicious Lesions: Evaluation of Breast Ultrasound, MRI Mammography and Electrical Impedance Scanning as Adjunctive Technologies in Breast Cancer Detection”, *Clinical Radiology*, pp: 278–283, v.56, 2001.
- [83] J. Marti, J. Batle, X. Cufi, J. Espanol, “Microcalcification evaluation in computer assisted diagnosis for digital mammography”, *Proceedings of the 1999 EE Colloquium on Digital Mammography*, pp: 1–6, 1999.
- [84] J. Marti, X. Cufi, J. Rgincos, J. Espanol, J. Pont, C. Barcelo, “Shape-based features selection for microcalcification evaluation”, *SPIE*, pp: 1215–1224, v. 3338, 1998.
- [85] T. Matsubara, T. Iuchikaw, T. Har, H. Fujit, S. Kasai, T. Endo, T. Iwase, “Automated Detection Methods for Architectural Distortions Around Skinline and Within Mammary Gland on Mammograms”. *International Congress Series*, pp: 950–955, v.1256, 2003.
- [86] D. Meersman, P. Scheunders, D.V. Dyck, “Classification of microcalcifications using texture-based features”, *Digital Mammography Nijmegen 1998*, pp: 233–236, 1998.
- [87] AJ. Mendez, Pablo G. Tahocesb, Maria J. Lado, Miguel Souto, Jose L. Correa, Juan J. Vidal, “Automatic Detection of Breast Border and Nipple in Digital Mammograms”, *Computer Methods and Programs in Biomedicine*, pp: 253–262, v.49, 1996.
- [88] Metin N. Gurcan, Heang-Ping Chan, PhD, Berkman Sahiner, PhD, Lubomir Hadjiiski, PhD, Nicholoas Petrick, PhD, Mark A. Helvie, MD, “Optimal Neural Network Architecture Selection: Improvement in Computerized Detection of Microcalcifications”, *Academic Radiology*, pp: 420–429, v.9, n.4, 2002.
- [89] C.E. Metz, “ROC methodology in radiologic imaging”, *Investigative Radiology*, pp: 720–733, v.21, 1986.
- [90] Mia K. Markey, Joseph Y. Lo, Georgia D. Tourassi, Carey E. Floud Jr. Self-Organizing “Map for Cluster Analysis of a Breast Cancer Database”, *Artificial Intelligence in Medicine*, pp: 113 – 127, v.27 (2003).
- [91] Michael A. Wirth, Alexei Stapinski, “Segmentation of the Breast Region in Mammograms Using Active Contours”, Dept. of Computing and Information Science, University of Guelph.
- [92] W.M. Morrow, R.B. Para jape, R.M. Rangayyan, J.E.L. Desautels, “Region-based contrast enhancement of mammograms”, *IEEE Trans. Med. Imag.*, pp: 392–406, v.11, n.3, 1992.
- [93] J.M. Mossi, A. Albiol, “Improving detection of clustered microcalcifications using morphological connected operators”, *IEEE Image Processing and its Applications*, pp: 498–501, 1999.
- [94] Naga R. Mudigonda, Rangaraj M. Rangayyan, Fellow, IEEE, and Leo Desautels J. E. “Detection of Breast Masses in Mammograms by Density Slicing and Texture Flow-Field Analysis”. *IEEE Transactions on Medical Imaging*, pp: 1215–1227, v.20, n.12, 2001.
- [95] T. Netsch, “A scale-space approach for the detection of clustered microcalcifications in digital mammograms, Digital Mammography’96”, *Proceedings of the Third International Workshop Digital Mammography, Chicago.*, pp: 301–306, 1996.
- [96] T. Netsch, H.O. Peitgen, “Scale-space signatures for the detection of clustered microcalcifications in digital mammograms”, *IEEE Trans. Med. Imag.*, pp: 774–786, v.18, n.9, 1999.
- [97] Nicholas Petrick, Member, IEEE, Heang-Ping Chan, Berkman Sahiner, Member, IEEE, and Datong Wei, “An Adaptive Density-Weighted Contrast

- Enhancement Filter for Mammographic Breast Mass Detection”, *IEEE Transactions on Medical Imaging*, v.15, n.1, 1996.
- [98] Nico Karssemeijer and Guido M. te Brake, “Detection of Stellate Distortions in Mammograms”, *IEEE Transactions on Medical Imaging*, pp: 611–619, v.15, n.5, 1996.
- [99] R.M. Nishikawa, M.L. Giger, K. Doi, C.J. Vyborny, R.A. Schmidt, “Computer-aided detection of clustered microcalcifications on digital mammograms”, *Med. Biol. Eng. Comput.*, pp: 174–178, v.33, n.2, 1995.
- [100] R.M. Nishikawa, Y. Jiang, M.L. Giger, K. Doi, C.J. Vyborny, R.A. Schmidt, “Computer-aided detection of clustered microcalcifications”, *Proceedings of the IEEE International Conference on Systems, Man and Cybernetics*, pp: 1375–1378, 1992.
- [101] R.M. Nishikawa, Y. Jiang, M.L. Giger, C.J. Vyborny, R.A. Schmidt, R. Bick, “Characterization of the mammographic appearance of microcalcifications: applications in computer-aided diagnosis”, *SPIE Image Process*, pp: 422–429, v.1898, 1993.
- [102] R.M. Nishikawa, M.L. Giger, K. Doi, C.J. Vyborny, R.A. Schmidt, “Computed-aided detection of clustered microcalcifications: an improved method for grouping detected signals”, *Med. Phys.*, pp: 1661–1666, v.20, n.6, 1993.
- [103] J.C. Olivo, “Automatic detection of spots in biological images by a wavelet-based selective filtering technique”, *Proceedings of the 1996 IEEE International Conference on Image Processing*, pp: 311–314, 1996.
- [104] N. Pandey, Z. Salcic, J. Sivaswamy, “Fuzzy logic based microcalcification detection”, *Neural Networks for Signal Processing—Proceedings of the IEEE Workshop 2*, pp: 662–671, 2000.
- [105] M. Pandey, S.P. Singh, P.B. Behere, S.K. Roy, S. Singh and V.K. Shukla, “Quality of Life In Patients With Early and Advanced Carcinoma of the Breast”, *European Journal of Surgical Oncology*, pp: 20–24, v.26, 2000.
- [106] A. Papadopoulos, D.I. Fotiadis, A. Likas, “An Automatic Microcalcification Detection System Based on a Hybrid Neural Network Classifier”, *Artificial Intelligence in Medicine*, pp: 149–167, v.25, 2002.
- [107] P. Pettazoni, G. Pallotti, G. Mattina, C. Leoni, “Computerized Detection of Clustered Microcalcifications: A Modular Approach with Nonlinear Filters”, *Medical Hypotheses*, pp: 442–447, 56, n.4, 2001.
- [108] F. Rafiee-Rad, H. Soltanina-Zadeh, M. Rahmati, S. Pour-Abdollah, “Microcalcification classification in mammograms using multiwavelet features”, *Proceedings of the 1999 Wavelet Applications in Signal and Image Processing*, pp: 832–841, 1999.
- [109] Reyer Zwiggelaar, Susan M. Astley, Caroline R.M. Boggis, and Christopher J. Taylor, “Linear Structures in Mammographic Images: Detection and Classification”, *IEEE Transaction on Medical Imaging*, pp: 1077–1086, v.23, n.9, 2004.
- [110] G.L. Rogova, P.C. Stomper, C. Ke, “Microcalcification texture analysis in a hybrid system for computer aided mammography”, *SPIE*, pp: 1426–1433, v.3661, 1999.
- [111] Rudy Setiono, “Extracting Rules from Pruned Neural Networks for Breast Cancer Diagnosis”, *Artificial Intelligence in Medicine*, pp: 37–51, v.8, 1996.
- [112] Rudy Setiono, “Generating Concise and Accurate Classification Rules for Breast Cancer Diagnosis”, *Artificial Intelligence in Medicine*, pp: 183–204, v.20, 2000.
- [113] Ruey-Feng Chang, Member, IEEE, Wen-Jie Wu, Chih-Chi Tseng, Dar-Ren Chen, and Woo Kyung Moon, “3-D Snake for US in Margin Evaluation for Malignant Breast Tumor Excision Using Mammotome”, *IEEE Transactions on Information Technology in Biomedicine*, pp: 197–201, v.7, n.3, 2003.
- [114] B. Sahiner, H.P. Chan, N. Petrick, M.A. Helvie, M.M. Goodsitt, “Design of a high-sensitivity classifier based on a genetic algorithm: application to computer-aided diagnosis”, *Phys. Med. Biol.*, pp: 2853–2871, v.43, 1998.
- [115] S. Sehad, S. Desarnaud, A. Strauss, “Artificial neural classification of clustered microcalcifications on digitized mammograms”, *Proceedings of the IEEE International Conference on Systems, Man and Cybernetics*, pp: 4217–4222, v.5, 1997.
- [116] L. Shen, R. Rangayyan, J.E.L. Desautels, “Detection and classification of mammographic calcifications”, *Int. J. Pattern Recognition Artif. Intell.*, pp: 1403–1416, v. 7, 1993.
- [117] Shuk-Mei Lai, Xiaobo Li, and Water F. Bischof, “On Techniques for Detecting Circumscribed Masses in Mammograms”, *IEEE Transactions on Medical Imaging*, pp: 377–386, v.8, n.4, 1989.
- [118] Shun Leung and Walter F. Bischof, “Automated Detection and classification of Breast Tumors”, *Computers and Biomedical Research*, pp: 218–337, v.25, 1992.
- [119] M.K.J. Siddiqui, M. Anand, P.K. Mehrotra, R. Sarangi, N. Mathur, “Biomonitoring of Organochlorines in Women with Benign and Malignant Breast Disease”, *Environmental Research*, pp: 1–8, 2004.
- [120] D. Song, W. Qian, L.P. Clarke, “Digital mammography: hybrid M-channel wavelet transform for microcalcification segmentation”, *18th Annual International Conference of the IEEE Engineering in*

- Medicine and Biology Society, Amsterdam*, pp: 1069–1070, 1996.
- [121] Stamatia Detounis, MD. “Computer-Aided Detection and Second Reading Utility and Implementation in a High-Volume Breast Clinic”, *Applied Radiology*, pp: 8–15, 2004.
- [122] R.N. Strickland, H.I. Hahn, L.J. Baig, “Wavelet methods for combining CAD with enhancement of mammograms”, *Medical Imaging 1996: Image Processing, SPIE Proceedings*, pp: 888–903, v.2710, 1996.
- [123] R.N. Strickland, H.I. Hahn, “Wavelet transform matched filters for the detection and classification of microcalcifications in mammography”, *Proceedings of the 1995 IEEE International Conference on Image Processing*, pp: 422–425.
- [124] R.N. Strickland, H.I. Hahn, “Wavelet transform methods for object detection and recovery”, *IEEE Trans. Image Process.*, pp: 724–735, v.6, 1997.
- [125] R.N. Strickland, H.I. Hahn, “Wavelet transforms for detecting microcalcifications in mammography”, *Proceedings of the International Conference on Image Processing, Austin, TX*, pp: 402–406, 1994.
- [126] R.N. Strickland, H.I. Hahn, “Wavelet transforms for detecting microcalcifications in mammograms”, *IEEE Trans. Med. Imag.*, pp: 218–229, v.15, n.2, 1996.
- [127] J.A. Swets, “ROC analysis applied to the evaluation of medical imaging techniques”, *Investigative Radiology*, pp: 109 – 121, v.14, 1979.
- [128] Sze Man Kwok, Ramachandran Chandrasekar, Member, IEEE, Yianni Attikiouzel, Fellow, IEEE, and Mary T. Rickard, “Automatic Pectoral Muscle Segmentation on Mediolateral Oblique View Mammograms”, *IEEE Transaction on Medical Imaging*, pp: 1129–1140, v.23, n.9, 2004.
- [129] Ted C. Wand and Nicolas B. Karayiannis, Member, IEEE. “Detection of Microcalcifications in Digital Mammograms Using Wavelets”, *IEEE Transactions on Medical Imaging*, pp: 498– 505, v.17, n.4, 1998.
- [130] Thomas Netsch and Heinz-Otto Peitgen, “Scale-Space Signatures for the Detection of Clustered Microcalcifications in Digital Mammograms”, *IEEE Transformations on Information Technology in Biomedicine*, pp: 774–786, v.18, n.9, 1999.
- [131] Thor Ole Gulsrud and John Hakon Husoy, “Optimal Filter-Based Detection of Microcalcifications”, *IEEE Transactions on Biomedical Engineering*, pp: 1272–1280, v.48, n.11, 2001.
- [132] Thor Ole Gulsrud, “Texture analysis of Digital Mammograms”, *Ph.D. Thesis*, pp: 30-32, 2000.
- [133] W.J.H. Veldkamp, N. Karssemeijer, “Normalization of local contrast in mammograms”, *IEEE Trans. Med. Imag.*, pp: 731–738, v.19, n.7, 2000.
- [134] B. Verma, “A neural network based technique to locate and classify microcalcifications in digital mammograms”, *IEEE International Conference on Neural Networks—Conference Proceedings*, pp: 1790–1793, v.3, 1998.
- [135] B.C. Wallet, J.L. Solka, C.E. Priebe, “A method for detecting microcalcifications in digital mammograms”, *J. Digital Imag.*, pp: 136–139, v.10, n.3 (1997).
- [136] Wei Qian, Laurence P. Clarke, Maria Kallergi, and Robert A. Clark, “Tree-Structured Nonlinear Filters in Digital Mammography”, *IEEE Transactions on Medical Imaging*, pp: 25–36, v.12, n.1, 1994.
- [138] Wojciech M. Grohman, Atam P. Dhawan, “Fuzzy Convex Set-Based Pattern Classification for Analysis of Mammographic Microcalcifications”, *Pattern Recognition*, pp: 1469–1482, v. 34, 2001.
- [139] K. Woods, C. Doss, K. Bowyer, L. Clarke, R. Clark, “A neural network approach to microcalcification detection”, *IEEE 1992 Nuclear Science Symposium and Medical Imaging Conference, Orlando, FL*, pp: 1273–1275, October 1992.
- [140] K.S. Woods, C.C. Doss, K.W. Bowyer, J.L. Sulk, C.E. Probe, W.P. Kegelmeyer, “Comparative evaluation of pattern recognition techniques for detection of microcalcifications in mammography”, *Int. J. Pattern Recognition Artif. Intell.*, pp: 1417–1436, v.7, 1993.
- [141] Y. Wu, K. Doi, M.L. Giger, R.M. Nishikawa, “Computer-aided detection of microcalcifications in digital mammograms”, *Invest. Radio.*, pp: 664–674, v.9, 1988.
- [142] Xiaolan Zeng, Sarah Medeiros, Susan A. Wood, Sandra Stapleton, Jimmy Roehrig, Kathryn O’Shaughnessy, Ronald A. Castellino, “Computer-Aided Detection for Mammography: Improved Algorithm Performance with Operator Determined Points Characterized By New Metrics”, *International Congress Series*, pp: 855–860, v.1268, 2004.
- [143] E. Yilmaz, B. Lebe, P. Balci, S. Sal, T. Canda, “Comparison of Mammographic and Sonographic Findings in Typical and Atypical Medullary Carcinoma of the Breast”, *Clinical Radiology*, pp: 640–645, v.57, 2002.
- [144] H. Yoshida, K. Doi, R.M. Nishikawa, “Automated detection of clustered microcalcifications”, *SPIE Image Processing*, pp: 868–886, v.2167, 1994.
- [145] H. Yoshida, W. Zhang, W. Cai, K. Doi, R.M. Nishikawa, M.L. Giger, “Optimizing wavelet transform based on supervised learning for detection of microcalcifications in digital mammograms”, *Proceedings of the IEEE International Conference on Image Processing*, pp: 152–155, v.3, 1995.
- [146] S. Yu, L. Guan, “A CAD system for the automatic detection of clustered microcalcifications in digitized mammogram films”, *IEEE Trans. Med. Imag.*, pp: 115–126, v.19, n.2, 2000.

- [147] S. Yu, L. Guan, S. Brown, "Automatic detection of clustered microcalcifications in digitized mammogram films", *J. Electron. Imag.*, pp: 76–82, v.8, n.1, 1999.
- [148] Yuji Hatanka, Tekeshi Hara, Hiroshi Fujita, Satoshi Kasai, Tokiko Endo, and Takuji Iwase, "Development of an Automated Method for Detecting Mammographic Masses with a Partial Loss of Region", *IEEE Transactions on Medical Imaging*, pp: 1209–1214, v.20, n.12, 2001.
- [149] H.S. Zadeh, S.P. Nezhad, F.R. Rad, "Shape-based and texture-based feature extraction for classification of microcalcification in mammograms", *Proc. SPIE*, pp: 301–310, v.4322, 2001.
- [150] L. Zhang, W. Qian, R. Sankar, D. Song, R. Clark, "A new false positive reduction method for MCCs detection in digital mammography", *IEEE International Conference on Acoustics, Speech and Signal Proc.*, pp: 1033–1036, 2001.
- [151] D. Zhao, M. Shridhar, D.G. Daul, "Morphology on detection of calcifications in mammograms", *IEEE International Conference on Acoustics, Speech and Signal Processing, III*, pp: 129–132, 1992.
- [152] B. Zheng, Y.H. Chang, Wang, W.F. Good, D. Gur, "Application of a Bayesian belief network in a computer-assisted diagnosis scheme for mass detection", *SPIE Conference on Image Processing, San Diego, CA*, pp: 1553–1560, v.3661, 1999.
- [153] B. Zheng, W. Qian, L.P. Clarke, "Digital mammography: mixed feature neural network with spectral entropy decision for detection of microcalcifications", *IEEE Trans. Med. Imag.*, pp: 589–597, v.15, n.5, 1996.

THANGAVEL KUTTIANNAN, received the Master of Science from Department of Mathematics, Bharathidasan University in 1986, and Master of Computer Applications Degree from Madurai Kamaraj University, India in 2001. He got his Ph. D.



Degree from Mathematics department, Gandhigram Rural Institute-Deemed University in 1999. Currently he is working as Reader in Mathematics Department, Gandhigram Rural Institute-Deemed University, and his experience started from 1988; His area of interests includes medical image processing, artificial intelligence, neural network, and fuzzy logic.

KARNAN MARCUS, received the Master of Computer Science and Engineering Degree from Computer Science and Engineering Department, from



Government College of Engineering, Manonmaniam Sundaranar University, Tamil Nadu, India, in 2000. Currently he is working as Assistant Professor, Department of Computer Science & Engineering Department, RVS

College of Engineering & Technology, Tamil Nadu, India. And doing part-time research in the Department of computer Science and Applications, Gandhigram Rural Institute-Deemed University, Tamil Nadu, India. His area of interests includes medical image processing, artificial intelligence, neural network, genetic algorithm, pattern recognition and fuzzy logic.

SIVA KUMAR RAMAKRISHNAN,. Received the Master of Computer Science and Engineering Degree



from Computer Science and Engineering Department, from Government College of Engineering, Manonmaniam Sundaranar University, Tamil Nadu, India, in 2000. Currently he is working as Assistant Professor,

Department of Computer Science & Engineering, RVS College of Engineering & Technology, Tamil Nadu, India. His area of interests includes medical image processing, artificial intelligence, neural network, and fuzzy logic.

KAJA MOHIDEEN ABUBAKKER, received the



Master of Computer Applications Degree from Computer Science Department, Bharathidasan University, Tamil Nadu, India, in 2000. Currently he is working as Research Assistant, in Department of Computer Science &

Engineering RVS College of Engineering & Technology, Tamil Nadu, India. His area of interests includes medical image processing, artificial intelligence, and neural network.

The following author designated as corresponding author:

Name: Karnan Marcus, E-mail id:

karnanme@yahoo.com, rsk_siva@mailcity.com, ktvel@rediffmail.com

Postal Address: 153, Palayam, Palani, Dindigul Dt, Tamil Nadu, India – 624601.

Fax.No:91-4551-227229,91-4551-227230,

Telephone.No:91-4551-227229,91-4551-2272.